Supplementary Information
"To bend or not to bend, the dilemma of multiple bonds"

M. Pizzochero[†], M. Bonfanti[‡] and R. Martinazzo[¶,§,*]

[†]Institute of Physics, Ecole Polytechnique Fédérale de Lausanne (EPFL), CH-1015 Lausanne, Switzerland

[‡]Institute of Physical and Theoretical Chemistry, Goethe Universität Frankfurt, Max-von-Laue-Str. 7, 60438 Frankfurt, Germany

[¶]Department of Chemistry, Università degli Studi di Milano, via Golgi 19, 20133 Milan, Italy

[§]Institute of Molecular Science and Technologies (ISTM), Consiglio Nazionale delle Ricerche (CNR), Milan, Italy

[*]E-mail: rocco.martinazzo@unimi.it

Note on this document

The sections of this document (that in the main article have been referenced as ESI:S1, ESI:S2, ESI:S3, etc.) are now labelled as Sec. S1, Sec. S2, Sec. S3, etc. Figures are referenced as Fig. F1,F2,F3, etc. and Tables as Tab. T1, etc. Page numbers are given as P1, P2, P3, etc..

S1 The Hubbard bond model

We detail in this section the results of the 2-state (or 2-site) Hubbard model that we used to describe bonding between two chemical species. We start from the general Hamiltonian in the second quantized form

$$H = \sum_{i,\sigma} \varepsilon_i a^\dagger_{i,\sigma} a_{i,\sigma} - t \sum_{\sigma} a^\dagger_{b,\sigma} a_{a,\sigma} +$$

$$- t \sum_{\sigma} a^\dagger_{a,\sigma} a_{b,\sigma} + \sum_i U_i n_{i,\uparrow} n_{i,\downarrow}$$

where σ runs over the spins ($\sigma = \uparrow, \downarrow$), i runs over the two lattice sites ($i = a, b$) and $a_{i,\sigma}$ ($a^\dagger_{i,\sigma}$) destroys (creates) an electron in state (orbital) i with spin σ, ε_i are the on-site energies and t is the hopping energy. We first consider the model for orthogonal orbitals and later address the problem of overlapping states. The problem is readily re-formulated in first quantization language where, for two electrons, H reads as

$$H = h_1 + h_2 + V$$

with h_l the monoelectronic operator for the l^{th} electron and V the Coulomb repulsion. The equivalence between the two is obtained upon setting

$$\langle a|h|a\rangle \approx \varepsilon_a \quad \langle b|h|b\rangle \approx \varepsilon_b$$

$$\langle a|h|b\rangle = \langle b|h|a\rangle = -t$$

$$\langle aa|V|aa\rangle = U_a \quad \langle bb|V|bb\rangle = U_b$$

and neglecting the remaining $e-e$ matrix elements. Here, $|a\rangle = a^\dagger_{a,\uparrow}|0\rangle$ (the choice of the spin is immaterial in the equations above) and $|aa\rangle = a^\dagger_{a,\uparrow} a^\dagger_{a,\downarrow}|0\rangle$ and similarly for $|b\rangle$ and $|bb\rangle$, $|0\rangle$ being the vacuum state. In such language the 2-electron wavefunction Ψ can be factorized into the product of a spatial (Φ) and a spin wavefunction (Θ), and the first becomes a combination of the following configurations (for the singlet ground-state)

$$\Phi_0 = \frac{1}{\sqrt{2}} \left(\phi_a(\mathbf{r}_1)\phi_b(\mathbf{r}_2) + \phi_b(\mathbf{r}_1)\phi_a(\mathbf{r}_2)\right)$$

$$\Phi_a = \phi_a(\mathbf{r}_1)\phi_a(\mathbf{r}_2) \quad \Phi_b = \phi_b(\mathbf{r}_1)\phi_b(\mathbf{r}_2)$$

i.e., a covalent configuration (Φ_0) and two ionic ones (Φ_a,Φ_b). It readily follows

H	$\lvert\Phi_0\rangle$	$\lvert\Phi_a\rangle$	$\lvert\Phi_b\rangle$
$\langle\Phi_0\rvert$	$\varepsilon_a+\varepsilon_b$	$-\sqrt{2}t$	$-\sqrt{2}t$
$\langle\Phi_a\rvert$	$-\sqrt{2}t$	$2\varepsilon_a+U_a$	0
$\langle\Phi_b\rvert$	$-\sqrt{2}t$	0	$2\varepsilon_b+U_b$

Symmetry (*i.e.*, whenever $a \leftrightarrow b$ under a symmetry operation of the Hamiltonian) makes the problem analytically solvable. Under such circumstances, indeed, only the even (or g) combination of ionic configurations,

$$\Phi_g = \frac{1}{\sqrt{2}} (\Phi_a + \Phi_b)$$

can interact with Φ_0 and the problem can be reformulated in this basis as

H	$\lvert\Phi_0\rangle$	$\lvert\Phi_g\rangle$
$\langle\Phi_0\rvert$	0	$-2t$
$\langle\Phi_g\rvert$	$-2t$	U

where we have set $\varepsilon_a = \varepsilon_b = 0$ and $U_a = U_b = U$. The ground-state energy then follows as

$$\varepsilon = \frac{U}{2} - \sqrt{\frac{U^2}{4} + 4t^2}$$

and the ground-state wavefunction as

$$\Phi = \Phi_0 + \left(\sqrt{1 + \frac{U^2}{16t^2}} - \frac{U}{4t} \right) \Phi_g$$

Upon defining the *transmission factor*

$$\xi = \sqrt{1 + \frac{U^2}{16t^2}} - \frac{U}{4t}$$

one re-writes the ground-state energy and wavefunction as

$$\boxed{\varepsilon = -2t\xi \quad \Phi = \Phi_0 + \frac{\xi}{\sqrt{2}} (\Phi_a + \Phi_b)}$$

where $E_b^{el} = -\varepsilon = 2t\xi$ is the electronic contribution to the *binding energy* [the repulsion energy between the ion cores can be subtracted at this point, if needed, to obtain the true binding energy]. When $U \ll t$ one finds that $\xi \to 1$ and

$$\varepsilon \approx -2t \quad \Phi \approx \frac{1}{\sqrt{2}}\left(\phi_a(\mathbf{r}_1)+\phi_b(\mathbf{r}_1)\right)\left(\phi_a(\mathbf{r}_2)+\phi_b(\mathbf{r}_2)\right)$$

This is the molecular orbital limit where the two electrons are paired in a molecular orbital and the bond energy attains its maximum value $2t$ (the factor of two is the number of electrons). On the other hand, when $U \gg t$ $\xi \to 0$ and the wavefunction takes a purely covalent form $\Phi \approx \Phi_0$ with a vanishing small binding energy $\sim 4t^2/U$. This is the Heitler-London (*aka* Heisenberg) limit, where the electrons reside on their nuclei in an entangled state. Here, the transmission factor ξ measures, in a sense, the "radical" character of the bond. To turn it into a "radical index" one can observe that $\xi^2/(1+\xi^2)$ is the weight of the ionic configurations (Φ_g), and thus a reasonable index could be $R_\xi = 1-2\xi^2/(1+\xi^2) \equiv (1-\xi^2)/(1+\xi^2)$, where the factor of two guarantees that $R_\xi = 0$ holds in the MO limit.

In general, the whole wavefunction, Ψ, can also be written in terms of (normalized) Slater determinants upon noticing that

$$\Psi_{a\bar{b}} - \Psi_{\bar{a}b} \equiv \sqrt{2}\Phi_0(\mathbf{r}_1,\mathbf{r}_2)\Theta^2_{0,0}(\sigma_1,\sigma_2)$$

where $|\Psi_{a\bar{b}}\rangle \equiv a^\dagger_{a,\uparrow}a^\dagger_{b,\downarrow}|0\rangle$, $|\Psi_{\bar{a}b}\rangle \equiv a^\dagger_{a,\downarrow}a^\dagger_{b,\uparrow}|0\rangle$ and Θ^N_{SM} is a normalized N-electron spin function with total spin S and projection M. Hence, one can also write

$$\Psi = \Psi_{a\bar{b}} - \Psi_{\bar{a}b} + \xi\left(\Psi_{a\bar{a}} + \Phi_{b\bar{b}}\right)$$

Alternatively, one can also use *polarized*, non-orthogonal orbitals

$$\psi_a(\mathbf{r}) = \phi_a(\mathbf{r}) + \eta\phi_b(\mathbf{r})$$

$$\psi_b(\mathbf{r}) = \phi_b(\mathbf{r}) + \eta\phi_a(\mathbf{r})$$

and write the exact ground-state wavefunction for this problem in a purely covalent form

$$\Psi \propto \left(\psi_a(\mathbf{r}_1)\psi_b(\mathbf{r}_2)+\psi_b(\mathbf{r}_1)\psi_a(\mathbf{r}_2)\right)\Theta^2_{0,0}$$

provided the *polarization factor* η is set to $(1-\sqrt{1-\xi^2})/\xi$. The latter is such that $\eta \to 1$ (0) in the molecular orbital (Heitler-London) limit, and captures the role of ionic configurations. Thus, such simple result shows that some care is needed in general when assessing the role of ionic structures.

The case of non-orthogonal states can be handled similarly. First, we define $S = \langle a|b\rangle = \langle b|a\rangle$,

$$\Phi_0 = \frac{1}{\sqrt{2(1+S^2)}}\left(\phi_a(\mathbf{r}_1)\phi_b(\mathbf{r}_2)+\phi_b(\mathbf{r}_1)\phi_a(\mathbf{r}_2)\right)$$

and Φ_a, Φ_b as above. The Hamiltonian matrix in the basis $\{\Phi_0, \Phi_1, \Phi_2\}$ then gets modified into

H	$\|\Phi_0\rangle$	$\|\Phi_a\rangle$	$\|\Phi_b\rangle$
$\langle\Phi_0\|$	$\frac{\varepsilon_a+\varepsilon_b-2tS}{1+S^2}$	$\sqrt{\frac{2}{1+S^2}}(\varepsilon_a S - t)$	$\sqrt{\frac{2}{1+S^2}}(\varepsilon_b S - t)$
$\langle\Phi_a\|$	$\sqrt{\frac{2}{1+S^2}}(\varepsilon_a S - t)$	$2\varepsilon_a + U_a$	$-2tS$
$\langle\Phi_b\|$	$\sqrt{\frac{2}{1+S^2}}(\varepsilon_b S - t)$	$-2tS$	$2\varepsilon_b + U_b$

while the overlap matrix reads as

1	$\|\Phi_0\rangle$	$\|\Phi_a\rangle$	$\|\Phi_b\rangle$
$\langle\Phi_0\|$	1	$\sqrt{\frac{2}{1+S^2}}S$	$\sqrt{\frac{2}{1+S^2}}S$
$\langle\Phi_a\|$	$\sqrt{\frac{2}{1+S^2}}S$	1	S^2
$\langle\Phi_b\|$	$\sqrt{\frac{2}{1+S^2}}S$	S^2	1

Note that, differently from the previous orthogonal case, the hopping energies here depend on the reference energy of the one-electron Hamiltonian h, that is usually set to be the asymptotic limit of the one-electron potential. Specifically, if we set $\bar{h} = h - \varepsilon_0$ we need the replacements

$$\varepsilon_a \to \bar{\varepsilon}_a = \varepsilon_a - \varepsilon_0$$

$$\varepsilon_b \to \bar{\varepsilon}_b = \varepsilon_b - \varepsilon_0$$

$$t \to \bar{t} = -\langle a|h-\varepsilon_0|b\rangle = t + \varepsilon_0 S$$

in order to recover the correct result $E \to \bar{E} = E - N\varepsilon_0$, where $N = 2$ is the number of electrons [In matrix notation, this follows of course from $\bar{\mathbb{H}} = \mathbb{H} - 2\varepsilon_0\mathbb{S}$ and the nature of the secular problem, which requires $\mathbb{S}E - \mathbb{H}$ to be singular].

As before, we focus on the symmetric case, set $\varepsilon_a = \varepsilon_b = 0$ and $U_a = U_b = U$ and introduce

$$\Phi_g = \frac{1}{\sqrt{2(1+S^2)}}\left(\Phi_a + \Phi_b\right)$$

This leads to

H	$\|\Phi_0\rangle$	$\|\Phi_g\rangle$
$\langle\Phi_0\|$	$-\frac{2\bar{t}S}{1+S^2}$	$-\frac{2\bar{t}}{1+S^2}$
$\langle\Phi_g\|$	$-\frac{2\bar{t}}{1+S^2}$	$\frac{U-2\bar{t}S}{1+S^2}$

and

1	$\|\Phi_0\rangle$	$\|\Phi_g\rangle$
$\langle\Phi_0\|$	1	$\frac{2S}{1+S^2}$
$\langle\Phi_g\|$	$\frac{2S}{1+S^2}$	1

and finally to the ground-state solution of the secular problem in the form

$$\varepsilon = \frac{4\bar{t}(1-S^2)S + U(1+S^2)}{2(1-S^2)^2} + \\ - \sqrt{\left[\frac{4\bar{t}(1-S^2)S+U(1+S^2)}{2(1-S^2)^2}\right]^2 + \frac{4\bar{t}^2 + 2\bar{t}S(U-2\bar{t}S)}{(1-S^2)^2}} \qquad (1)$$

In this expression $\bar{t}$ is understood to be the hopping energy computed with the one-electron operator referenced to ε_a, *i.e.*, $\bar{t} = t + \varepsilon_a S$ where t and ε_a are matrix elements of the original, not-shifted Hamiltonian.

Eq. 1 generalizes the one obtained above under the (stringent) constraint of vanishing overlap orbital which, though, remains very useful for interpretative purposes. For instance, by analogy,

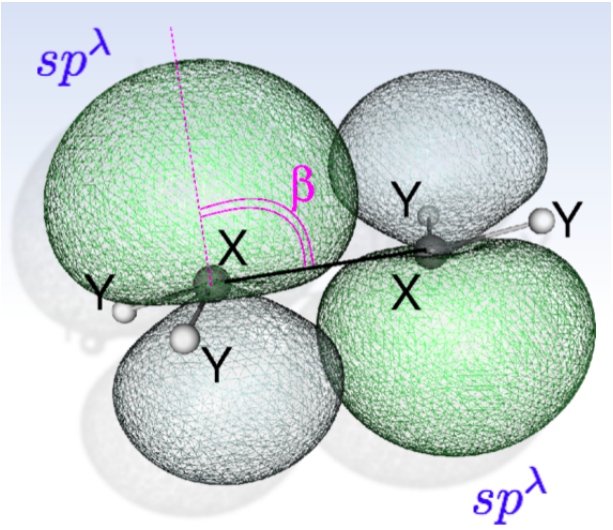

Fig. F1 Schematics of the C_{2h} configuration considered for describing binding in a Y_2X=XY_2 molecule, illustrating the sp^λ used for the π bond, together with the angle β that they make with the XX axis. The central atoms X use further sp^τ and sp^μ hybrids for the XY and XX σ bonds.

one can now define an effective transmission factor as

$$\xi_{\rm eff} = -\varepsilon/2|\bar{t}|$$

and obtain an effective U/t ratio as

$$(U/t)_{\rm eff} = \frac{2\left(1-\xi^2\right)}{\xi}$$

The latter can also be expressed in terms of effective radical character, $R_{\rm eff} = (1-\xi_{\rm eff}^2)/(1+\xi_{\rm eff}^2)$, as

$$(U/t)_{\rm eff} = \frac{4R_{\rm eff}}{\sqrt{1-R_{\rm eff}^2}}$$

S2 The $\sigma+\pi$ Hubbard double bond

We apply the above Hubbard model *separately* to the σ- and π-like bonds of a (possibly distorted) Y_2X=XY_2 molecule, focusing on symmetric C_{2h} configurations (the case of a triple bond YX≡XY can be handled similarly provided an out-of-plane π bond is factored out at the outset). To this end we assume that the two X atoms make a non-bent σ-bond using sp^μ hybrids, while they form the π-like bond with the help of sp^λ hybrids, leaving two further hybrids sp^τ available for the XY bonds (equivalent to each other in C_{2h} symmetry, see Fig. F1). We shall discuss later the relationship between the hybridization indexes μ,λ and the molecular geometry.

The sp^μ and sp^λ hybrids determine the overlap matrix elements, and the effective hopping and Coulomb on-site energies to be used in the Hubbard-bond model, namely $S_\sigma^{eff}, t_\sigma^{eff}, U_\sigma^{eff}$ for the σ bond and $S_\pi^{eff}, t_\pi^{eff}, U_\pi^{eff}$ for the π one. They also determine the on-site energies (*i.e.* the expectation values of the one-electron Hamiltonian operator), but these are mostly irrelevant in the present model since in a total energy comparison, together with the sp^τ contributions, they just give a constant (geometry independent) energy term - the energy of the atomic sp^3 configuration - that can be safely neglected.

We start by addressing the problem of the one-electron matrix elements involved in the σ bond. The two orbitals involved in the bond are sp^μ hybrids of the form

$$|\phi_a\rangle = \frac{1}{\sqrt{1+\mu}}\left(|s\rangle + \sqrt{\mu}\,|p\rangle\right)$$

$$|\phi'_a\rangle = \frac{1}{\sqrt{1+\mu}}\left(|s'\rangle + \sqrt{\mu}\,|p'\rangle\right)$$

where unprimed (primed) orbitals are centered on the first (second) atom, and $|p\rangle, |p'\rangle$ are *directional* p orbitals oriented from their center to the other atom. The main quantities of interest here are the effective overlap and the hopping energy

$$S_\sigma^{eff} = \langle\phi_a|\phi_b\rangle\,,\; t_\sigma^{eff} = -\langle\phi_a|h|\phi_b\rangle$$

the Coulomb energy will be addressed below. Expanding these matrix elements in terms of atomic orbital contributions we get

$$\boxed{S_\sigma^{eff} = \frac{1}{1+\mu}\left\{S_\sigma(ss) - 2\sqrt{\mu}S_\sigma(sp) - \mu S_\sigma(pp)\right\}}$$

$$\boxed{t_\sigma^{eff} = \frac{1}{1+\mu}\left\{t_\sigma(ss) - 2\sqrt{\mu}t_\sigma(sp) - \mu t_\sigma(pp)\right\}}$$

with the following common definitions for AO matrix elements

$$S_\sigma(ss) = \langle s|s'\rangle\,,\; S_\sigma(sp) = \langle s|p'_X\rangle$$

$$S_\sigma(pp) = \langle p_X|p'_X\rangle\;\; t_\sigma(ss) = -\langle s|h|s'\rangle$$

$$t_\sigma(sp) = -\langle s|h|p'_X\rangle\,,\; t_\sigma(pp) = -\langle p_X|h|p'_X\rangle$$

where X denotes the XX bond axis. Notice that, according to the AO orientation, it holds $t_\sigma(ss), S_\sigma(ss) \geq 0$ while $t_\sigma(sp), S_\sigma(sp), t_\sigma(pp), S_\sigma(pp) \leq 0$.

Next, we turn attention to the π-bond, for which the relevant sp^λ hybrids use $|p\rangle$ and $|p'\rangle$ orbitals at an angle β with the XX axis, see Fig. F1. If Z is the axis along the symmetry plane, orthogonal to the bond axis, we have

$$|p\rangle = \cos\beta\,|p_X\rangle + \sin\beta\,|p_Z\rangle$$

$$|p'\rangle = -\cos\beta\,|p'_X\rangle - \sin\beta\,|p'_Z\rangle$$

and, thus, with the usual definitions $S_\pi^{eff} = \langle\phi_a|\phi_b\rangle$, $t_\pi^{eff} = -\langle\phi_a|h|\phi_b\rangle$, it follows

$$\boxed{\begin{aligned} S_\pi^{eff} \;&= \tfrac{1}{1+\lambda}\Big\{S_\sigma(ss) - 2\sqrt{\lambda}\cos\beta S_\sigma(sp) + \\ &\quad -\lambda\left(\cos^2\beta S_\sigma(pp) + \sin^2\beta S_\pi(pp)\right)\Big\}\end{aligned}}$$

$$\boxed{\begin{aligned} t_\pi^{eff} \;&= \tfrac{1}{1+\lambda}\Big\{t_\sigma(ss) - 2\sqrt{\lambda}\cos\beta t_\sigma(sp) + \\ &\quad -\lambda\left(\cos^2\beta t_\sigma(pp) + \sin^2\beta t_\pi(pp)\right)\Big\}\end{aligned}}$$

Here, according to the AO orientations, it holds $S_\sigma(ss)$, $S_\pi(pp)$, $t_\sigma(ss)$, $t_\pi(pp) \geq 0$ and $S_\sigma(sp)$, $S_\sigma(pp)$, $t_\sigma(sp)$, $t_\sigma(pp) \leq 0$. Notice

further that in the limit of planar configurations ($\beta \to \pi/2$), for distortions that preserve C_{2h} symmetry, we have $\lambda \to \infty$, $S_\pi^{eff} \to -S_\pi(pp)$ and $t_\pi^{eff} \to -t_\pi(pp)$, consistently with the direction of the π-like orbitals.

Finally, we consider the *bare* Coulomb energy

$$U_\nu^0 = \langle \psi_\nu \psi_\nu | V | \psi_\nu \psi_\nu \rangle$$

for a generic sp^ν hybrid ($\nu = \mu, \lambda$ for U_σ^{eff} and U_π^{eff} respectively). Expanding U_ν in terms of AO contributions and keeping only the classical terms we obtain

$$U_\nu^0 \approx \frac{1}{(1+\nu)^2} U_{ss} + \frac{2\nu}{(1+\nu)^2} U_{sp} + \frac{\nu^2}{(1+\nu)^2} U_{pp}$$

This latter expression, as well as the above ones for $t_\sigma^{eff}, S_\sigma^{eff}$, etc., can also be conveniently written in terms of $s-$weights in the sp^ν hybrids, $w_\nu = 1/(1+\nu)$, *i.e.*, in the form

$$\boxed{U_\sigma^{eff,0} \approx w_\mu^2 U_{ss} + 2w_\mu(1-w_\mu)U_{sp} + (1-w_\mu)^2 U_{pp}}$$

$$\boxed{U_\pi^{eff,0} \approx w_\lambda^2 U_{ss} + 2w_\lambda(1-w_\lambda)U_{sp} + (1-w_\lambda)^2 U_{pp}}$$

These are bare quantities that only apply to unscreened orbitals; more appropriate quantities are the *screened* ones, that account for the effect of the remaining electrons on the ones singled out for describing the bond. We generally write

$$U_\sigma^{eff} = U_\sigma^{eff,0}/\varepsilon_\sigma \quad U_\pi^{eff} = U_\pi^{eff,0}/\varepsilon_\pi$$

where ε_k ($k = \sigma, \pi$) are effective dielectric constants for the σ and π electrons, as given *e.g.* in the constrained random-phase-approximation[1]. For the π electrons, for instance, one has

$$U_\pi = (1 - U^0 P_r)^{-1} U^0$$

where $P_r = P - P_\pi$, P is the total (typically frequency-dependent) polarization, P_π is the polarization of the π electrons, U^0 is the bare Coulomb interaction and U_π is the screened one appropriate for π electrons. Upon taking matrix elements between π orbitals one then finds the appropriate expression for ε_π.

These screening constants are generally geometry-dependent, in a way that only actual calculations can reveal. However, for the sake of modeling, we write $\varepsilon = \varepsilon_q \varepsilon_{cl}$ where ε_{cl} is the classical permittivity of a mixture of s and p "media",

$$\varepsilon_{cl} = w_\nu \varepsilon_s + (1 - w_\nu)\varepsilon_p$$

ε_s, ε_p being the permittivities appropriate for s and p orbitals and w_ν the $s-$weight in the hybrid considered. Such orbital contributions can be obtained from different sources. For instance, calculations on π-conjugated systems give the p contributions, which can be combined with information on sp^ν hybrids on simple molecular systems to obtain the s ones. We use the triplet-singlet vertical separation energy in XH_2 since, consistently with a Hubbard-like description of bonding, it is given by (see Sec. S5)

$$E_{TS} = w_\nu \Delta - U_n$$

where Δ is the $s-p$ separation energy, U_n is the effective Coulomb energy in the $n-$like hybrid of the singlet and w_ν the weight of the s component in such hybrid. As for the "cooperative" contribution ε_q, we do not expect much for the σ bonds ($\varepsilon_q \approx 1$, irrespective of pyramidalization), while for the π bonds we expect on physical grounds that ε_q increases somewhat when molecular pyramidalization occurs, since screening is at minimum in the planar configuration (2D-like system).

To close this section we remember that, in our model, the above (geometry-dependent) effective parameters enter in the energy expression for the σ and the π bond energies, *e.g.,* in the limit of vanishing orbital overlaps, it holds

$$\varepsilon_\sigma = -2|t_\sigma^{eff}|\xi_\sigma \;\; \xi_\sigma = \sqrt{1 + \frac{\left(U_\sigma^{eff}\right)^2}{16\left(t_\sigma^{eff}\right)^2}} - \frac{U_\sigma^{eff}}{4|t_\sigma^{eff}|}$$

and

$$\varepsilon_\pi = -2|t_\pi^{eff}|\xi_\pi \;\; \xi_\pi = \sqrt{1 + \frac{\left(U_\pi^{eff}\right)^2}{16\left(t_\pi^{eff}\right)^2}} - \frac{U_\pi^{eff}}{4|t_\pi^{eff}|}$$

[In the non-orthogonal case one would use Eq. 1 with $\tilde{t}_\pi^{eff} = t_\pi^{eff} + \varepsilon_\lambda S_\pi^{eff}$ for the π bond and $\tilde{t}_\sigma^{eff} = t_\sigma^{eff} + \varepsilon_\mu S_\sigma^{eff}$ for the σ one]. These equations give a simple expression for the energy of the $\sigma + \pi$ bond

$$E = \varepsilon_\sigma + \varepsilon_\pi + v(R)$$

(where $v(R)$ is a short-range potential that accounts for the repulsion between the X ion cores) and thus the bond energy can be written as

$$E_{\sigma+\pi} = E_\sigma + E_\pi - v(R)$$

where $E_\nu = -\varepsilon_\nu$ ($\nu = \sigma, \pi$). By construction, this bond energy is referenced to the *triplet* state of the fragments and is the binding (or "cohesive") energy of the system (E_{BE}) w.r.t. the fragment separation only when XY_2 has a triplet ground-state. When it is not the case, $E_{\sigma+\pi}$ must be corrected for the promotion energy needed to excite the fragments into their triplet state

$$E_{BE} = E_{\sigma+\pi} - \Sigma E_{TS}$$

where $E_{TS} = E_T - E_S$ is the triplet-singlet separation energy of each fragment, and Σ stands for their sum ($\Sigma E_{TS} \equiv 2E_{TS}$ in the symmetric case considered here). It is obvious that no $\sigma+\pi$ bonding scheme can be conceived when $E_{\sigma+\pi} < \Sigma E_{TS}$.

Finally, notice that in order to define separate $\sigma-$ and $\pi-$ bond energies it is necessary that the core potential is attributed to one of the two bonds, or split among them. Since the π bond can be broken while keeping the σ intact, one reasonably defines E_π as the "π bond energy" and $E_\sigma - v(R)$ as the "σ bond energy".

S3 Fractional hybridization

Determining the nature of the hybrid orbitals involved in a π bonded X=X system becomes a straightforward geometrical exercise if one assumes that the X atoms form non-bent σ bonds with the substituents using some kind of sp^ν hybrids. Indeed, from the

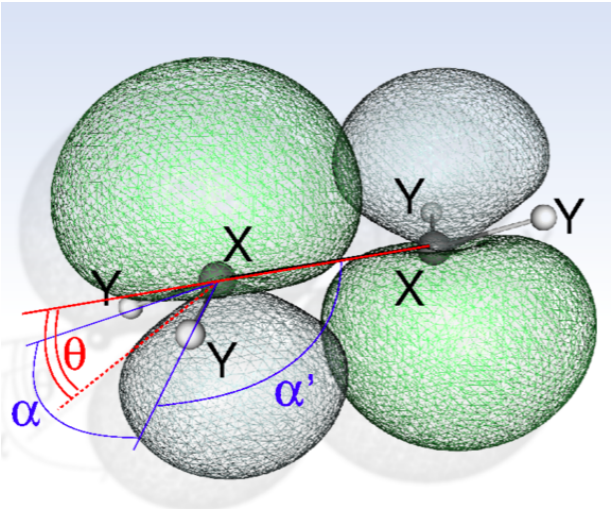

Fig. F2 Schematics of a $Y_2X{=}XY_2$ molecule in C_{2h} symmetry illustrating the main structural parameters.

orthogonality constraint between (unnormalized) hybrids

$$|\psi_\nu\rangle = |s\rangle + \sqrt{\nu}\,|p\rangle$$

it follows

$$\langle\psi_\nu|\psi_{\nu'}\rangle = 1 + \sqrt{\nu\nu'}\cos\theta_{\nu\nu'}$$

where $\theta_{\nu\nu'}$ is the corresponding bond angle (Coulson's directionality theorem). For the problem at hand of a $Y_2X{=}XY_2$ molecule in C_{2h} symmetry we take the hybrids to be sp^τ for the XY bonds and sp^μ for the XX σ bond. The *hybridization indexes* τ,μ then follow as

$$\boxed{\tau = -\frac{1}{\cos\alpha}}$$

and

$$\sqrt{\mu} = -\frac{1}{\sqrt{\tau}\cos\alpha'}$$

or, equivalently,

$$\boxed{\mu = -\frac{\cos\alpha}{\cos^2\alpha'}}$$

where α and α' are the YXY and YXX angles, respectively (see Fig. F2). More generally, for three σ bonds directed along $\hat{\mathbf{n}}_1,\hat{\mathbf{n}}_2$ and $\hat{\mathbf{n}}_3$, the corresponding indexes τ_i follow as

$$\boxed{\tau_i = -\frac{\hat{\mathbf{n}}_j\hat{\mathbf{n}}_k}{(\hat{\mathbf{n}}_i\hat{\mathbf{n}}_j)\,(\hat{\mathbf{n}}_i\hat{\mathbf{n}}_k)}}$$

where $i,j,k = 1,2,3$ $(i\neq j\neq k)$. [Note that this is a rather unique situation where the number of hybridization indexes matches that of independent angles. For instance, for the two τ, μ hybridization indexes needed to describe the YX and XX σ bonds in YX≡XY the bond angle ∠YXX is the only geometrical parameter available. On the other hand, for the four indexes needed in XY_4 (at an arbitrary configuration) the six independent bond angles are too many for the four indexes, and the non-bent bond assumption must be lifted].

Having defined three hybrids (out of four basis functions) the fourth one, say sp^λ - that is also the one involved in the π-bond - follows easily by either analytical or geometrical considerations. Let $\hat{\mathbf{n}}$ be the unit axis along such hybrid, $g_i = \hat{\mathbf{n}}\hat{\mathbf{n}}_i = -1/\sqrt{\lambda\tau_i}$ and $\mathbf{A}$ the symmetric matrix of elements $A_{ij} = \hat{\mathbf{n}}_i\hat{\mathbf{n}}_j$. If $\hat{\mathbf{n}}_i$ are not co-planar, $\hat{\mathbf{n}}$ can be expanded as $\hat{\mathbf{n}} = \sum_i c_i\hat{\mathbf{n}}_i$ and easily seen to give $\mathbf{Ac} = \mathbf{g}$ (where $\mathbf{c}$ and $\mathbf{g}$ are column vectors with components c_i and g_i, respectively) and $\hat{\mathbf{n}}\hat{\mathbf{n}} = 1 = \mathbf{c}^t\mathbf{Ac}$, *i.e.*, $1 = \mathbf{g}^t\mathbf{A}^{-1}\mathbf{g}$. On the other hand, upon defining $\mathbf{t}$ the vector of components $t_i = -1/\sqrt{\tau_i}$ it also holds $\sqrt{\lambda}\mathbf{g} = \mathbf{t}$. Hence, under such circumstances, it follows at once

$$\lambda = \mathbf{t}^t\mathbf{A}^{-1}\mathbf{t}$$

while $\arccos(-1/\sqrt{\lambda\tau_i})$ $(i = 1-3)$ give the directional angles that the hybrid makes with the σ bonds. When the latter are co-planar $\mathbf{A}$ is singular, λ is infinite and the directional angles are $\pi/2$, as expected.

Alternatively, the hybridization index λ can be obtained by the conservation of the s (or p) weights upon hybridization, namely from

$$1 = \mathrm{Tr}P \equiv \sum_i w_{\tau_i} + w_\lambda$$

where $w_\nu = 1/(1+\nu)$ is the $s-$weight in the sp^ν hybrid, $P = |s\rangle\langle s|$ is the projector on the $s-$shell and, in the rightmost equivalence, the trace over the sp manifold has been evaluated on the set of (normalized) hybrids. In other words, it holds

$$\lambda = \frac{1}{1-\sum_i(1+\tau_i)^{-1}} - 1$$

which is explicitly singular for co-planar σ bonds. In the specific case we are interested in, a convenient measure of the "distortion" of the π-axis is given by the angle that the hybrid makes with the XX bond, namely

$$\beta = \arccos\left(\cos\alpha'\sqrt{-\frac{1}{\lambda\cos\alpha}}\right)$$

Such "orbital" axis needs to be distinguished from the geometrical pyramid axis $\hat{\mathbf{k}}$, defined by the condition $\hat{\mathbf{k}}\hat{\mathbf{n}}_1 = \hat{\mathbf{k}}\hat{\mathbf{n}}_2 = \hat{\mathbf{k}}\hat{\mathbf{n}}_3 \equiv \cos\gamma$, where γ can be considered as the "pyramid angle". They both measure the deviation from a planar arrangement, but with different aims. The first relies on the hybrization of the central atom, the second is based exclusively on the molecular structure. For the latter, simple geometrical arguments give

$$\cos\gamma = \frac{1}{\sum_{ij}(\mathbf{A}^{-1})_{ij}}$$

where $\mathbf{A}$ is the previously defined matrix of direction cosines.

Most often, though, one uses a different (geometrical) measure of pyramidalization, namely the angle θ that the XX bond makes with the plane of YXY′ bonds, the so-called pyramidalization angle (Fig. F2). For a generic configuration one readily finds,

$$\cos\theta = \sqrt{\cos^2\alpha_3 + \frac{(\cos\alpha_3\cos\alpha_1 - \cos\alpha_2)^2}{\sin^2\alpha_1}}$$

where $\alpha_1,\alpha_2,\alpha_3$ are, respectively, the YXY′, Y′XX and XXY angles.

For the symmetric C_{2h} cases ($\alpha_2=\alpha_3\equiv\alpha'$, $\alpha_1\equiv\alpha$) one obtains

$$\boxed{\cos\theta=-\frac{\cos\alpha'}{\cos\left(\frac{\alpha}{2}\right)}}$$

S4 *Trans*-bending: model results

It is possible to analyze to some extent the behaviour of the $\sigma+\pi$ bond strength upon *trans*-bending. To this end we focus on a planar, D_{2h} configuration and bend the molecule (decrease the angle α') while keeping the angle α frozen at the value it takes in the planar configuration (see Fig. F2). This guarantees that the sp^τ orbitals used for the XY σ bonds remain unchanged upon bending and, thus, that the energy variations refer only to the $\sigma+\pi$ bond system. We first consider the effective π hopping energy t_π^{eff} (similar results follow for the effective overlap, S_π^{eff}) and rewrite it in the form

$$t_\pi^{eff}=\frac{1}{1+\lambda}\left\{t_\sigma(ss)+\right.$$
$$\left.-\frac{2}{\sqrt{\mu}}t_\sigma(sp)-\lambda t_\pi(pp)+\frac{1}{\mu}\left[t_\pi(pp)-t_\sigma(pp)\right]\right\}$$

where $\lambda\cos^2\beta\equiv\mu^{-1}$ has been used to replace the directional angle β with the hybridization index μ of the XX bond. Next, we introduce $\delta\eta=\lambda^{-1}$ to discuss the behaviour of this matrix element for *quasi*-planar configurations, $\delta\eta\approx 0$ and, after some simple algebra, we get

$$\frac{|t_\pi^{eff}(\theta)|}{|t_\pi^{eff}(0)|}=\frac{1}{1+\delta\eta}\left\{1+\right.$$
$$\left.-\delta\eta\left[\frac{1}{\mu}\left(1+r(pp)\right)+\frac{2}{\sqrt{\mu}}r(sp)+r(ss)\right]\right\}$$

where θ is the pyramidalization angle and the *positive* quantities $r(pp),r(sp)$ and $r(ss)$ are the $pp(\sigma)$, $sp(\sigma)$ and $ss(\sigma)$ hopping energies in units of the π one, *i.e.*, $r(pp)=|t_\sigma(pp)|/|t_\pi(pp)|$, $r(sp)=|t_\sigma(sp)|/|t_\pi(pp)|$ and $r(ss)=|t_\sigma(ss)|/|t_\pi(pp)|$. Note that it is manifestly a decreasing function of $\delta\eta$, *i.e.* of the pyramidalization angle. More precisely, from the $s-$weight sum

$$\frac{2}{1+\tau}+\frac{1}{1+\mu}+\frac{1}{1+\lambda}=1$$

it follows[N6] that $\mu_*=2/(\tau-1)$ is the value that μ takes in the planar configuration, and that

$$\delta\mu=\mu-\mu_*\approx(1+\mu_*)^2\delta\eta$$

N6 It is not hard to show that this amounts to the statement that $\alpha'=\alpha/2$ must hold in the planar configuration.

Hence, to first order in $\delta\eta$, it holds

$$\frac{|t_\pi^{eff}(\theta)|}{|t_\pi^{eff}(0)|}=1+$$
$$-\delta\eta\left[1+\frac{1}{\mu_*}\left(1+r(pp)\right)+\frac{2}{\sqrt{\mu_*}}r(sp)+r(ss)\right]$$

This expression also shows that, for fixed r's, the decrease of t_π^{eff} with θ is faster the smaller μ_* is or, equivalently (remember that $\mu_*=2/(\tau-1)$ and $\tau=-1/\cos\alpha$), the smaller the α angle is. According to Bent's rule, such an increased tendency towards small YXY (equilibrium) angles can be obtained when increasing the Y's electronegativity.

As for the effective Coulomb energy, we notice that the bare matrix element is explicitly a decreasing function of pyramidalization since, to first order in the s-weight of the sp^λ hybrid ($w_\lambda\equiv\delta\eta/(1+\delta\eta)$), we have

$$U_\pi^{eff,0}\approx U_{pp}-2w_\lambda\left(U_{pp}-U_{sp}\right)$$

where $U_{pp}>U_{sp}$ holds on physical grounds. Screening adds a further decreasing contribution since, as already mentioned above, it is expected that the effective dielectric constant ε_π is an increasing function of w_λ, being at its minimum in the planar (2D-like) configuration.

As for the σ bond, the effective Coulomb energy is typically an increasing function of pyramidalization, since $U_\sigma^{eff}(\theta)\approx U_\sigma^{eff}(0)+\frac{dU_\sigma^{eff}}{dw_\mu}(0)\delta w_\mu$ where $\delta w_\mu<0$ (pyramidalization moves some s weight of the sp^μ hybrid into the π-like one, sp^λ) and

$$\frac{dU_\sigma^{eff}}{dw_\mu}(0)\equiv 2w_{\mu_*}(U_{ss}+U_{pp}-2U_{sp})+2(U_{sp}-U_{pp})\lesssim 0$$

since the last term on the r.h.s. usually dominates the sum. As for the hopping energy, an analysis similar to the one given above for t_π^{eff} shows that also $t_\sigma^{eff}(\theta)$ is a decreasing function of θ, since it holds

$$\frac{t_\sigma^{eff}(\theta)}{t_\sigma^{eff}(0)}\approx 1-\delta\mu\left[\frac{1}{\mu_*+1}-\frac{|t_\sigma(sp)|/\sqrt{\mu_*}+|t_\sigma(pp)|}{t_\sigma^{eff}(0)}\right]$$

where the second term in the square bracket is much smaller than $(1+\mu_*)^{-1}\approx 1/3$. However, for the σ bond orbital overlap cannot be neglected and the appropriate hopping energy to look at is that corrected for the overlap factor, $\bar{t}_\sigma^{eff}=t_\sigma^{eff}+\varepsilon_\mu S_\sigma^{eff}$, where ε_μ is the energy of the sp^μ orbital. Numerical calculations with realistic values of the parameters (see below) show that such overlap factor is important and changes this predicted trend, making $\bar{t}_\sigma^{eff}(\theta)/\bar{t}_\sigma^{eff}(0)$ actually *increasing* when increasing the pyramidalization angle. In turn, since in the MO limit typically appropriate for the σ bond the behaviour of U is irrelevant, this finding suggests that *the σ bond is strengthened upon distortion*. This contrasts with *the decrease of the π hopping energy* that, in the same limit, *would provide* a *restoring force toward the planar configuration*. In practical situations (see below), the weakening of the π bond is observed for a wide range of internuclear distances, even though the MO limit does *not* apply to the π-bond. As a consequence, Coulomb repulsion plays yet a role and weakens (strengthens) such restoring force when increasing (decreasing) the U_π^{eff}/t_π^{eff} ratio, *e.g.*, when π donor (acceptor) Y groups are introduced or when stretching (compressing) the bond. It is actually straightforward to check that, in the HL limit, provided

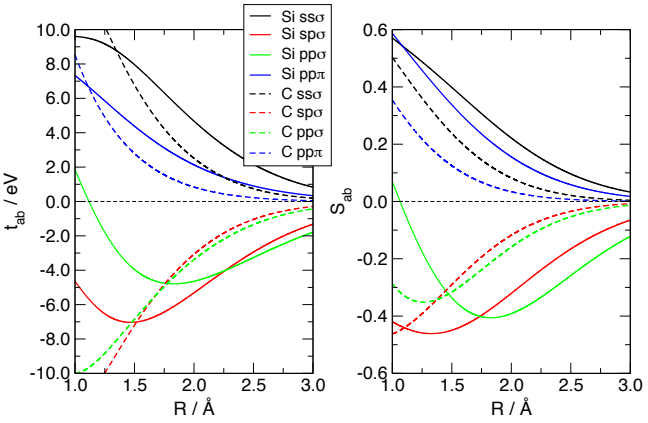

Fig. F3 Hopping (left) and overlap (right) parameters in homonuclear atom pairs, as functions of the interatomic distances. Results from *first-principles* calculations of Ref.s[2,3]. Solid and dashed lines for Si and C, respectively.

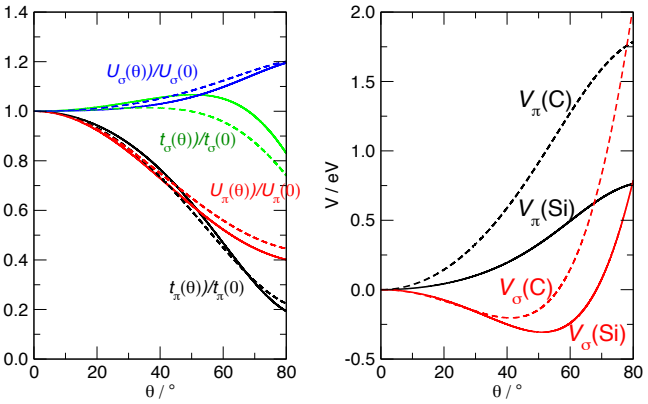

Fig. F4 Typical behaviour of the effective matrix elements upon bending (left) and corresponding energy contributions to the bending potential (right), using hopping and overlap parameters appropriate for X=Si,C at the equilibrium bond length and HXH angle in $H_2X{=}XH_2$ (see text for details). θ is the pyramidalization angle of Fig. F2.

U_π^{eff} decreases sufficiently fast with θ, the π bond can even be *strengthened* upon pyramidalization.

At a more quantitative level, the behaviour of the effective overlap and effective hopping and Coulomb energies as functions of the pyramidalization angle θ can be investigated numerically for reasonable values of the fundamental parameters $t_\sigma(ss), S_\sigma(ss), ..U_{ss}, ..$, etc..

In practice, the *bare* Coulomb energies are atomic quantities that can be obtained from reasonably accurate valence s and p orbitals. We used Slater-type orbitals and found, *e.g.*, that U_{pp} takes the values U_{pp} =18.3, 13.3 and 11.9 eV for C, Si and Ge atoms, while U_{ss} takes smaller values, U_{ss} =17.0,12.3 and 10.9 eV, for the same atoms, respectively. Screening can be introduced easily at a classical level (see Sec. S2), using appropriate permittivities for the s and p orbitals, ε_s and ε_p. For carbon, cRPA calculations on the p atomic orbitals in graphene[4] give $\varepsilon_p \approx 1.8$, while from the vertical triplet-singlet separation energy in $CH_2(^1A_1)$ ($\angle$HCH $\approx 102°$, $n \sim sp^{1.6}$) we obtain $\varepsilon_s \approx 2.2$. For silicon, similar cRPA calculations for silicene[4] give ≈ 2.78, but this value refers to $\pi-$like AOs rather than pure p orbitals, because buckling of the silicene sheet implies some admixture with s orbitals. We find that such orbitals are indeed $\sim sp^{10.1}$ hybrids, and together with a vertical $SiH_2(^1A_1)$ triplet-singlet separation of 1.27 eV, and the fact that the $n-$like orbital in $SiH_2(^1A_1)$ is $\sim s$ ($\angle$HSiH $\approx 91°$) we obtain $\varepsilon_s \approx \varepsilon_p \approx 2.8$. For the sake of modeling, ε_q was then taken $\equiv 1$ for the σ bond, and to be a simple increasing function of the $s-$weight in the sp^λ hybrid for the π bond ($\varepsilon_q = (1+w_\lambda)^2$).

The one-particle matrix elements $t_\pi(pp)$, $S_\pi(pp)$, etc. on the other hand, depend on the distance between the two atoms and were taken from Ref.[2] for the C-C pair and from Ref.[3] for the Si-Si one. They were obtained from scratch from *first-principles* calculations as one-particle matrix elements between properly compressed atomic orbitals, that are appropriate for atoms in a binding environment. They were represented analytically by means of Chebyshev polynomials and are shown in Fig. F3 in a range of interatomic distances relevant for binding.

We used the above parameters to compute the binding energy given by our $\sigma+\pi$ Hubbard bond model (Eq. 1), exploring a wide range of situations. Fig. F4, left panel, shows the typical behaviour upon *trans*-bending of the effective Hubbard parameters $\bar{t}_k^{eff}, U_k^{eff}$ ($k=\sigma,\pi$) for both silicon (solid lines) and carbon (dashed lines). They were obtained at the B3LYP/6-31++G** bond length of H_2XXH_2 ($R_{XX}=2.18, 1.33$ for X=Si,C), fixing $\alpha = \angle$HXH to its equilibrium value ($\alpha = 111.67, 116.5°$ for X=Si,C), but look very similar over a broad range of XX distances and α angles. As anticipated above, pyrmidalization decreases the (magnitude) of the effective $\bar{t}$, U for the π bond, while it increases their values for the σ bond. This holds for both Si and C. Actually, the relative variations of the parameters do not show significant differences in passing from Si to C [even the $\theta=0$ $U_k/\bar{t}_k$ ratios take similar values $\sim 1.0, 4.5$ for $k=\sigma,\pi$ for both Si and C], the only exception being $\bar{t}_\sigma$ that increases more for Si than for C, when increasing θ, on account of the (relatively) major importance that $pp(\sigma)$ hopping has for Si (see also Fig. F6). Notice, though, that a more appropriate comparison requires the calcula-

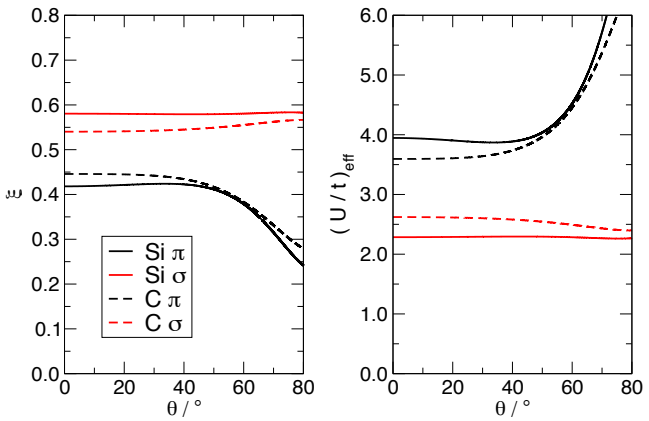

Fig. F5 Left: transmission factors for the Si-Si (solid lines) and the C-C (dashed lines) double bonds at their equilibrium distances. Black and red lines for the π and the σ bond, respectively. Right: corresponding U/t effective ratios, color coded as in the left panel.

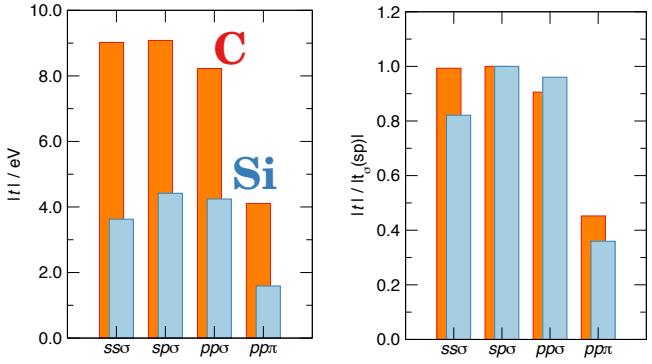

Fig. F6 Magnitude of the hopping parameters for Si and C at the equilibrium bond length in H_2XXH_2 (left). In the right panel the values are given relative to the σ sp one to highlight the different relative importance that $t_\sigma(ss)$ has for Si and C.

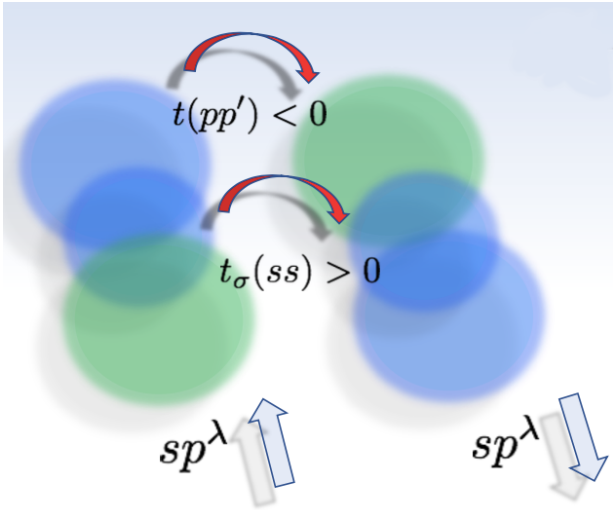

Fig. F7 Schematics showing the destructive interference between $ss(\sigma)$ and $pp(\pi)$ hoppings. Here, p and p' are two p orbitals centered on the two X atoms and directed along the pyramid axes (for a C_{2h} configuration of Y_2XXY_2). Note that, by convention, t's are minus the one-particle matrix elements, and thus display the same sign as the overlap matrix elements.

tion of the *effective* transmission factors and *effective* (U/t) ratios, that, in a sense, account for the non-vanishing overlap between the hybrids (Sec. S1). These are given in Fig. F5 for both the σ and the π bonds, where a clear difference emerges between the two types of bonds and, to a much lesser extent, between the two atoms. What is readily evident from Fig. F5 is that while the σ bond keeps its "character" when bent, the π one is rather sensitive to the bending (pyramidalization) angle and, besides its weakening, it undergoes a clear change of character beyond $\sim 50^\circ$, for both C and Si. As for the two atoms, $(U/t)_{\rm eff}$ remains very similar between Si and C, just slightly larger for the former than for the latter (at $\theta = 0$ we find ~ 3.9 and ~ 3.6 , respectively), consistently with the results of the cRPA calculations of Wehling *et al.*[4] on the π−like orbitals in silicene and graphene (~ 4.2 and ~ 3.6, respectively). Note the differences between $(U/t)_{\rm eff}$ and the "true" $U/\bar{t}$ ratios quoted above (particularly for the σ bond) that highlights the importance of the orbital overlap.

The subtle difference between Si and C arises from the relative importance of σ and π binding, that is different for the two atoms. For $\theta = 0$ we find that the ratio E_π/E_σ is slightly larger for C than for Si (0.22 *vs.* 0.18), and this makes π bonding more important for C. As a consequence, π bond opposes more effectively to pyramidalization in C than in Si. This is made evident in Fig. F4, right panel, where the contributions V_σ and V_π to the bending potential $V(\theta) = v(R,\theta) - v(R,0)$ are reported for H_2SiSiH_2 (solid lines) and H_2CCH_2 (dashed lines) at the XX equilibrium distance and $\alpha = \angle$HXH angle quoted above. The corresponding total bending potentials are reported as black lines in Fig. F9, in the left panel for X=Si and in the right one for X=C, and show a *trans*-bent minimum for Si and a flat one for C, in agreement with *first-principles* results (a comparison with *ab initio* results will be presented below). It is clear from Figs. F4,F9 that for both X=Si and C the σ bond triggers pyramidalization and the π bond opposes to it, but only for carbon the π restoring force is large enough to prevent distortion.

The relative importance of π *vs.* σ bond strength is one important cause for the different behaviour of C and Si, but it cannot be the only one. After all, it is the bending stiffness of the π bond, rather than its strength, that determines its resistance and, with the same token, it is the hardening of the σ bond rather than its strength that provides the driving force to bending. Figures F6,F7 and F8 provides a detailed overview of the contributing hopping energies at equilibrium XX separation. Fig. F6 shows both the absolute (left panel) and the relative (to $t_\sigma(sp)$, right panel) values of the basic hopping energies and highlights the main differences between the two atoms: for C both the $pp(\pi)$ and the $ss(\sigma)$ hoppings are easier than for Si, and these factors both contribute to make distortion unfavoured. In this context, the role of the $ss(\sigma)$ hopping deserves some consideration, since it is somewhat counter-intuitive: while its role on σ bonding is as expected, a larger $ss(\sigma)$ hopping energy seems to favor a *strengthening* of the π bond upon bending, rather than a weakening. The reason why this is not the case is made evident in Fig. F7, where it is shown that the $ss(\sigma)$ hopping path interferes *destructively* with the $pp(\pi)$ hopping, thereby determining a weakening of the π bond upon distortion, which is larger the larger $t_\sigma(ss)$ is. Actually, it is readily seen in Fig. F8 that if $t_\sigma(ss)$ for CC bonding had the same minor importance that it has for SiSi ($t_\sigma(ss) \sim 0.8|t_\sigma(sp)|$) a *trans*-bent minimum would occur for H_2CCH_2 too.

Fig. F9 shows that the effect of the YXY angle is such to increase bending when decreasing the angle, *i.e.*, when increasing the hybridization index of the sp^τ orbitals involved in the XY σ bonds (or, equivalently, decreasing the index μ of the orbitals used for XX binding). As mentioned above, the YXY angle can be related through Bent's rule to the electronegativity of the substituent Y, hence this figure shows that increasing the Y electronegativity facilitates distortion. Analysis of the separate π and σ contributions (Fig. F10) reveals that Y's electronegativity increases both the σ bond strengthening upon distortion and the π bond "stiffness" (as anticipated by the analytical results given above, when discussing the dependence of $\bar{t}_\pi$ on μ_*) but the first prevails on the latter.

Fig. F11 shows the effect of the π Coulomb energy on pyra-

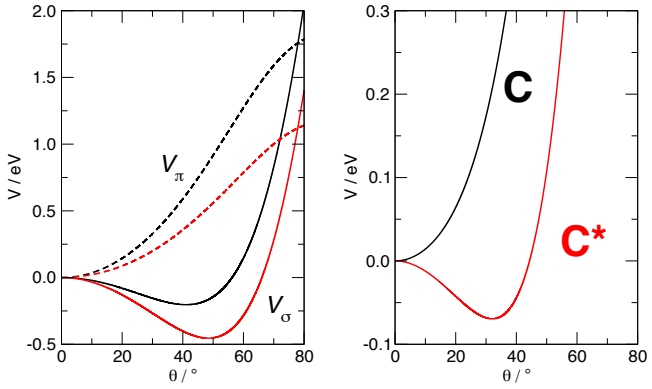

Fig. F8 Bending potential in real (black) and fictitous (red) H_2CCH_2 with a *reduced* $ss(\sigma)$ hopping energy (see text for details). Left: σ and π bending potentials. Right: total bending potential.

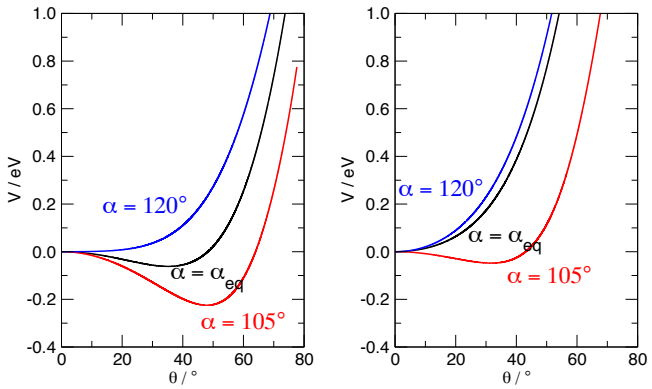

Fig. F9 Full bending potential similar to Fig. F4, for different values of the α angle. Left and right panels for Si and C, respectively.

midalization. This energy is an atomic-like quantity that only depends on the nature of the X atom, but can be used as a surrogate to mimic the behaviour of π-donor or π-acceptor substituents Y that, increasing or decreasing the effective number of π electrons, make Coulomb repulsion more or less important [in fact a more appropriate modeling of the $\sigma+\pi$ bond would require the fully machinery of second-quantized formalism that, allowing for fractional numbers of electrons, is able to discuss properly the $\sigma+\pi$ open electronic system]. We just consider two limits, that set upper and lower bounds for the role of π donating/accepting substituents: the case of vanishing small (blue lines) and of infinitely large (red lines) Coulomb energies. The results shown in Fig. F11 for both Si (left panel) and C (right) are as expected: decreasing (increasing) U_π^{eff} strengthens (weakens) the π bond, that thus opposes better (worse) to pyramidalization. In other words, our simple modeling shows that π-acceptors (donors) make distortion less (more) facile. Note that the case $U_\pi^{eff}=0$ corresponds to a simple tight-binding modeling, and Fig. F11 shows that such level of theory is *not* enough to reproduce the pyramidalization predicted for H_2SiSiH_2 by both post-Hartree-Fock and density functional theory calculations.

Finally, Fig.s F12, F13 show the effect of the XX distance on *trans*-bending. Stretching the XX bond decreases the strength of both σ and π bonding but, importantly, it makes the π bond less effective in opposing to bending (because of the increased U_π/t_π ratio). As a consequence, a bent structure is predicted for H_2CCH_2 for CC distances larger than the equilibrium one, while a flat structure is found for H_2SiSiH_2 when decreasing the SiSi distance below its equilibrium value. In this context it is worth analyzing in some detail the role of the $\pi-$resistance and of the $\sigma-$force to bending. This can be accomplished by looking at the curvatures at $\theta=0$ of the corresponding contributions to the bending potential, namely $y_\pi=d^2V_\pi/d\theta^2|_{\theta=0}$ and $y_\sigma=-d^2V_\sigma/d\theta^2|_{\theta=0}$, for the π and the σ bond, respectively. These quantities can be given in a physically sound form by introducing an appropriate cartesian coordinate, a "buckling" coordinate h that describes the distortion. To this end, we introduce one dummy hydrogen point mass in the bisection of each YXY angle, 1 Å away from the closest X, and define the buckling coordinate as $h=Z_*-Z'_*$, where Z_* and Z'_* are the Z coordinates of these dummy atoms (the Z coordinate has been introduced in Sec. S1). The corresponding π and σ frequencies - what we have called "$\pi-$bending stifness" and "$\sigma-$bending moment" in the main article - then read as $\omega_\pi=\sqrt{y_\pi/4m_Hd^2}$ and $\omega_\sigma=\sqrt{y_\sigma/4m_Hd^2}$, where $d=1$ Å, m_H is the hydrogen mass and $h\approx 2\theta d$ (for $\theta\approx 0$) has been used. They are reported in Fig. F13, where it is evident that it is the behaviour of the $\pi-$bending stiffness that mainly determines the distortion, the $\sigma-$moments being of similar magnitude for Si and C and showing a less marked dependence on the distance. Such $\pi-$stiffness is *larger* for Si at any XX distance but rapidly decreases with increasing R. As a result, the one for C at the CC equilibrium distance is larger than the one for Si at the SiSi equilibrium distance, and this allows the π bond to resist to bending. We stress again in this context the importance of the $ss(\sigma)$ hopping that for C is comparatively larger than for Si: it is the destructive interference between this hopping and the $pp(\pi)$ one (Fig. F7) that makes the carbon $\pi-$bending stiffness large enough and the CC double bond flat.

Overall, the findings reported in Fig. F12 are in remarkable good agreement with the results of our *first-principles* calculations reported in Fig. 1d - especially in light of the very simple nature

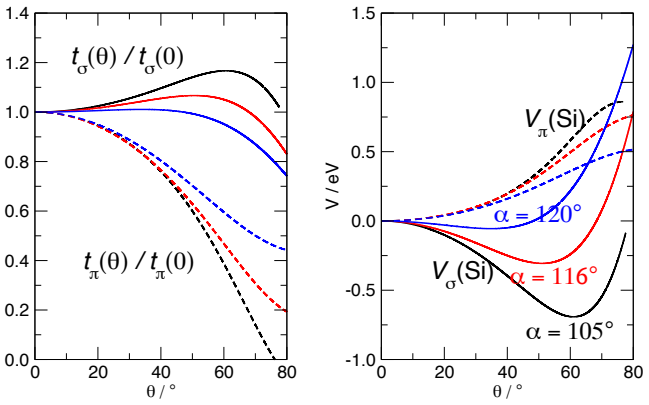

Fig. F10 Left: effective σ (solid lines) and π (dashed lines) hopping energies $\bar{t}$ in H_2SiSiH_2 as a function of pyramidalization, for different values of the HSiS angle, $\alpha=105,116$ and 120 (black, red and blue, respectively). Right: corresponding σ and π bending potentials.

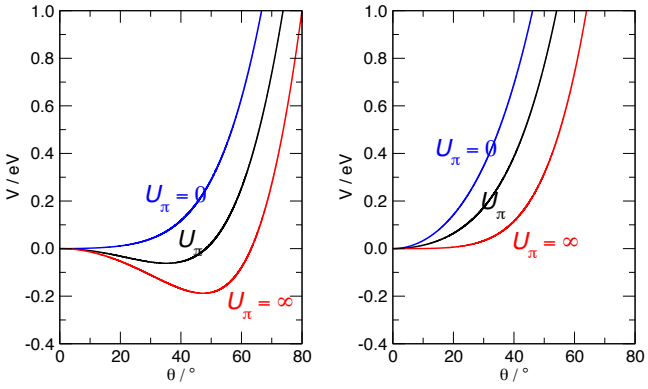

Fig. F11 Effect of the π Coulomb repulsion for Si (left panel) and C (right). Blue and red lines represent the opposite limits of vanishing and infinite on-site Coulomb energies, while black lines use the values discussed in the main text for modeling H_2SiSiH_2 and H_2CCH_2.

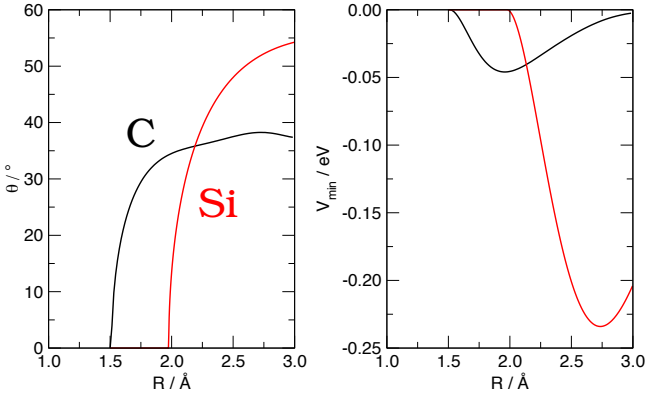

Fig. F12 Left: equilibrium pyramidalization angle θ as a function of the XX distance in Y_2XXY_2, for X = C and Si, using values of $\alpha = \angle YXY$ appropriate for Y = H. Right: corresponding bending energy at minimum.

of our model - except maybe for an "anticipated" distortion of H_2CCH_2, for which the critical distance at which distortion occurs is ~ 1.5 Å in the model rather than ~ 1.9 Å as in the DFT results. The discrepancy is due to the rather flat energetics of H_2CCH_2 that is found in both the model and the *first-principles* calculations and that is hard to capture with precision (see Fig. 3). Actually, the overall bending energetics compares rather favorably with the more sophisticated calculations (Fig. 3d), thereby lending strong support to the validity of our modeling. Further comparison with *ab initio* calculations will be presented below where we discuss an alternative way of binding that is potentially at work when the fragments have a singlet ground-state.

S5 The $n \to p$ double bond model

We describe here an alternative way of binding in $Y_2X{=}XY_2$, the "$n \to p$ bonding scheme", that might become relevant when the triplet-singlet separation of the fragment $E_{TS} = E_T(XY_2) - E_S(XY_2)$ is positive and sufficiently large that the $\sigma+\pi$ bond energy ($E_{\sigma+\pi}$) is not enough to compensate the promotion energy $2E_{TS}$ that is necessary to prepare the fragments in the triplet state (*i.e.*, the bonding configuration for the traditional $\sigma+\pi$ double bond). In the $n \to p$ bonding scheme the two fragments make two identical, bent bonds using the (doubly occupied) n orbital of one fragment and the (empty) p orbital of the other fragment, both in their singlet ground state (see Fig. F14). The actual nature of these orbitals depends on the specific choice of X: using Natural Bond Orbital (NBO) analysis[5] at the B3LYP/6-31++G** level we find, for instance, that the n orbital in the singlet $^1A_1$ state of CH_2 (with a bond angle of 102°) is approximately $sp^{1.6}$, while in SiH_2 (bond angle 91°) is essentially pure s.

In view of the above, we write the total energy as $\varepsilon = 2\varepsilon_{np}$ where ε_{np} is the Hubbard energy of a single $n \to p$ bond. The latter follows by the general Hamiltonian given above and reads as

H	$\lvert\Phi_0\rangle$	$\lvert\Phi_n\rangle$	$\lvert\Phi_p\rangle$
$\langle\Phi_0\rvert$	$\frac{\varepsilon_n+\varepsilon_p-2tS}{1+S^2}$	$f_S(\varepsilon_n S - t)$	$f_S(\varepsilon_p S - t_{np})$
$\langle\Phi_a\rvert$	$f_S(\varepsilon_n S - t_{np})$	$2\varepsilon_n + U_n$	$-2t_{np}S$
$\langle\Phi_b\rvert$	$f_S(\varepsilon_p S - t_{np})$	$-2t_{np}S$	$2\varepsilon_p + U_p$

where $f_S = \sqrt{2/(1+S^2)}$, ε_n (ε_p) and U_n (U_p) are atomic-like quantities (*i.e.*, the n (p) orbital and Coulomb energies, respectively) and $\lvert\Phi_n\rangle$,$\lvert\Phi_p\rangle$ are the n^2, p^2 ionic configurations. t_{np} and S, on the other hand, are the effective $n-p$ hopping energy and overlap, and depend on the binding geometry. In the above expression, consistently with a Hubbard description of binding, $2\varepsilon_n + U_n$ is the singlet energy of the XY_2 fragment (E_S) and $\varepsilon_n + \varepsilon_p$ is the triplet one (E_T); hence, the triplet-singlet separation can be expressed in terms of the $s-p$ separation energy ($\Delta \equiv \varepsilon_p - \varepsilon_s$) and the $s-$weight of the $n-$like orbital (w_{μ_*}) as $E_{TS} = w_{\mu_*}\Delta - U_n$, with $E_{TS} \le w_{\mu_*}\Delta$ if U_n has to be a positive quantity. Setting $\varepsilon_n = 0$ and neglecting the p^2 configuration (we are interested in the case of large E_{TS} values) we write the secular matrix in the form

$\varepsilon_{np} - H$	$\lvert\Phi_0\rangle$	$\lvert\Phi_n\rangle$
$\langle\Phi_0\rvert$	$\varepsilon - \frac{E_T - 2\bar{t}_{np}S}{1+S^2}$	$\sqrt{\frac{2}{1+S^2}}(\varepsilon S + \bar{t}_{np})$
$\langle\Phi_a\rvert$	$\sqrt{\frac{2}{1+S^2}}(\varepsilon S + \bar{t}_{np})$	$\varepsilon - E_S$

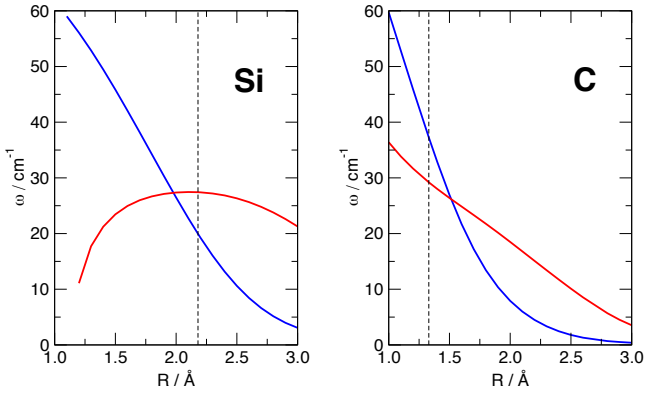

Fig. F13 Bending stiffness of the π bond (blue) and moment of the σ one (red) for Si (left panel) and C (right panel), as functions of the XX distance. Dashed vertical lines mark the equilibrium bond lengths.

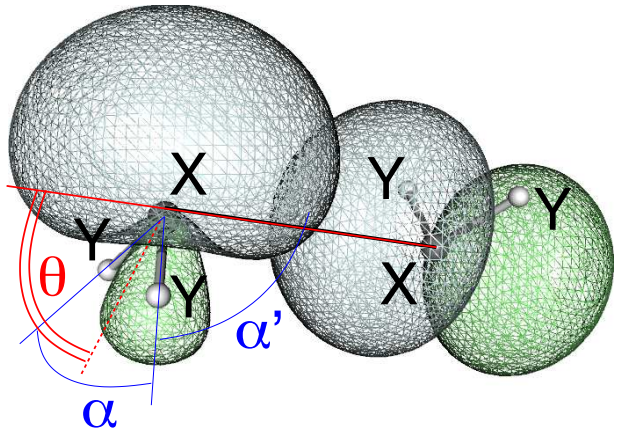

Fig. F14 Schematics of the $n \to p$ double model in Y_2X=XY_2, showing the $n-$like orbital on the left XY_2 fragment and the $p-$like orbital on the right one.

and readily find that it is singular for

$$\varepsilon_{np} = \varepsilon_0 - \sqrt{\varepsilon_0^2 + \frac{2\bar{t}_{np}^2 - E_S(E_T - 2\bar{t}_{np}S)}{(1-S^2)}}$$

where

$$\varepsilon_0 = \frac{(1+S^2)E_S + E_T + 2\bar{t}_{np}S}{2(1-S^2)}$$

and where now $\bar{t}_{np}$ is understood to be the $n-p$ hopping referenced to ε_n, $\bar{t}_{np} \equiv t_{np} + \varepsilon_n S$. This result takes a simple form when neglecting the overlap,

$$\varepsilon_{np} = \frac{E_S + E_T}{2} - \sqrt{\frac{E_{TS}^2}{4} + 2t_{np}^2}$$

and gives the total $n \to p$ double-bond energy in the form

$$\varepsilon = E_S + E_T - \sqrt{E_{TS}^2 + 8t_{np}^2}$$

that can be compared with that obtained from the $\sigma+\pi$ bonding scheme

$$\varepsilon = 2E_T - E_{\sigma+\pi}$$

The only *caveat* is that such an independent electron pair description of $n \to p$ binding completely neglects exchange effects. In particular a "Pauli repulsion" is operative at small pyramidalization angles θ when $E_{TS} > 0$, because of the overlap between the two $n-$type orbitals that essentially host two electrons each (for a given X-X distance such Pauli repulsion is at maximum for $\theta = 0$ where two orbitals face each other, and decreases with increasing θ). This repulsion modifies the $\theta \approx 0$ energetics but does *not* affect the minimum region around $\theta = 45°$ in which we are interested, hence it can be reasonably modeled by a term proportional to the magnitude of the $n-n$ overlap (S_{nn}).

In the expressions above t_{np} (and similarly for S) is the hopping matrix element between the $n-$like orbital of one XY_2 fragment with the p orbital of the other one. The first is coplanar with the two hybrids sp^τ used for the XY bonds, hence it is a hybrid

$$|\psi_n\rangle = \frac{1}{\sqrt{1+\mu_*}}\left(|s\rangle + \sqrt{\mu_*}\,|p\rangle\right)$$

where $\mu_* = 2/(\tau - 1)$ (see discussion above) and $|p\rangle$ is a directional p orbital lying on the YXY plane. The latter reads as

$$|p\rangle = \cos\theta\,|p_X\rangle + \sin\theta\,|p_Z\rangle$$

where θ is the pyramidalization angle, X is the XX bond axis and Z is othogonal to it (it reduces to the π axis when $\theta = 0$). On the other hand, the p orbital on the other fragment can be taken of the form

$$|\psi'_p\rangle = -\sin\theta\,|p'_X\rangle + \cos\theta\,|p'_Z\rangle$$

where now the primed orbitals refer to the opposite fragment. Hence, after some simple algebra we obtain

$$\boxed{\begin{aligned} t_{np}^{eff} &= -\tfrac{1}{1+\mu_*}\{t_\sigma(sp)\sin\theta + \\ &+\sqrt{\mu_*}\,(t_\sigma(pp) - t_\pi(pp))\sin\theta\cos\theta\} \end{aligned}}$$

where $t_\sigma(sp), t_\sigma(pp) \le 0$ and $t_\pi(pp) \ge 0$, and likewise

$$\boxed{\begin{aligned} S_{np}^{eff} &= -\tfrac{1}{1+\mu_*}\{S_\sigma(sp)\sin\theta + \\ &+\sqrt{\mu_*}\,(S_\sigma(pp) - S_\pi(pp))\sin\theta\cos\theta\} \end{aligned}}$$

where $S_\sigma(sp), S_\sigma(pp) \le 0$ and $S_\pi(pp) \ge 0$.

We used these expressions, with the overlap and hopping energies introduced above, to compute the pyramidalization energetics of this $n \to p$ bonding scheme and compared the results with those of the $\sigma+\pi$ model, as well as of *first-principles* calculations (the B3LYP/6-31++G** results discussed in Sec. S6). Such a comparison is presented in Fig. F15 where the energy as a function of the pyramidalization angle is reported for several values of the Si-Si distance R_{SiSi}, referenced to the singlet-singlet asymptote $2SiH_2(^1A_1)$, at its equilibrium structure ($\angle$HSiH = 91°). As before, pyramidalization has been followed at fixed $\alpha = \angle$HSiH angle in disilene ($\alpha = \alpha_{eq}$ =111.67°), but now the short-range, repulsive Si-Si potential of Ref.[3] (the "ionic" potential term) has been added to make the comparison with *ab initio* results possible (in addition, as mentioned above, for $n \to p$ binding we added a "Pauli repulsive potential", $V_P \propto |S_{nn}|$, that only affects the energetics at small angles). Fig. F15 shows that $n \to p$ binding is indeed competitive with standard $\sigma+\pi$ binding, with energies similar or even smaller than $\sigma+\pi$ at large θ. The model overemphasizes *trans*-bending but it is surely worth considering when discussing pyramidalization in H_2SiSiH_2. In particular, one sees from Fig. F15 that its contribution is marginal at small (close to equilibrium) SiSi distances (left panel in Fig. F15), but becomes more and more important when increasing R_{SiSi}. For $R_{SiSi} \sim R_{eq}$ $n \to p$ binding is favored over $\sigma+\pi$ only for $\theta \gtrsim 60°$ where it shapes the repulsive wall and makes it less steep than the one predicted by the $\sigma+\pi$ model, as observed in the DFT calculations. A more refined treatment of bonding would likely require an interaction between the two $n \to p$ and the $\sigma+\pi$ structures, but this seems to be not relevant for the equilibrium structure of H_2SiSiH_2. On the contrary, at larger R_{SiSi} distances (see, *e.g.*, the case $R_{SiSi} = 3.00$ Å reported in green in the right panel of the same figure) $n \to p$ binding dominates over $\sigma+\pi$, and the

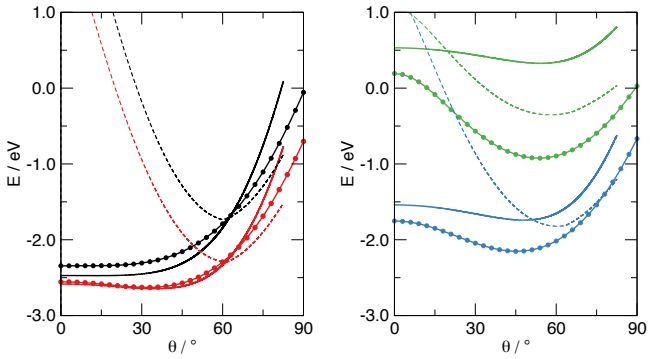

Fig. F15 Pyramidalization energetics in model and in *ab initio* calculations for H_2SiSiH_2, at fixed $\alpha = 111.67°$, referenced to the singlet-singlet asymptote (see text for details). Solid and dashed lines for the results of the $\sigma+\pi$ and $n-p$ models, respectively, and lines with symbols for B3LYP/6-31++G** *first-principles* data. Left panel for $R_{SiSi} = 2.00$ Å (black) and for $R_{SiSi} = R_{eq} = 2.18$ Å(red). Right panel for $R_{SiSi} = 2.50$ Å (blue) and $R_{SiSi} = 3.00$ Å (green).

predicted bending curves agree much better to the results of our *first-principles* calculations to support the view that at such large SiSi distances interaction is best described as dative bonds between two bent singlet fragments.

Finally, Fig. F16 reports the results of a similar comparison for H_2CCH_2. Again, energies are referenced to the singlet-singlet asymptote $2CH_2(^1A_1)$ at its equilibrium structure ($\angle HCH = 102°$) (which is now an excited state, since $E_{TS} < 0$ for CH_2) and pyramidalization has been followed at the equilibrium $\angle HCH$ angle in ethylene ($\alpha = \alpha_e = 116.5°$). As expected, for X = C the $\sigma+\pi$ bonding model is more "robust" and the alternative $n \to p$ double-bond, though lying at surprisingly low energies, is always higher in energy for a rather wide range of C-C distances. Only for $R_{CC} \gtrsim 2.50$ Å the $n \to p$ double bond becomes really competitive with $\sigma+\pi$ but, as for H_2SiSiH_2 above, a *trans*-bent minimum is already appearent at shorter distances in $\sigma+\pi$ model results, in agreement with the *first-principles* calculations.

In closing this section, we stress once again the remarkable agreement between the results of our model and the DFT data, that is really impressive in light of the simplicity of the model.

S6 *Trans*-bending: *first-principles* results

We present here the results of some detailed *first-principles* calculations focused on the $n \to p$ binding scheme suggested long ago by Trinquier and Malrieu[6–8] that has found widespread use since its introduction. The DFT calculations were performed as indicated in Sec. S10.

Fig. F17 shows disilene energetics along the clever path devised by Trinquier and Malrieu[6] to investigate pyramidalization. From the right to left, the two silylenes are first brought to the equilibrium distance in an orthogonal bent geometry (step 1), then recover planarity through *trans*-bending (step 2), the whole motion keeping a C_{2h} symmetry (Fig. F17a). In step 1 the profile is expected to be rather flat when the fragments are in the singlet state (which is the ground-state for SiH_2) because two empty p orbitals face each other, while only a $pp(\sigma)$ interaction is allowed when they are in the triplet (the first excited state) and this involves the two p orbitals orthogonal to the HSiH planes, the remaining two p electrons being left unpaired. Upon bending, the "triplet-triplet" state becomes strongly interacting because of pairing (and rearrangement) of the latter two e, while the "singlet-singlet" one becomes attractive because of $n \to p$ bonding. Whether the latter dominates over the first a *trans*-bent geometry naturally occurs because $n \to p$ bonding is at its maximum for $\theta \sim 45°$.

In our calculations we considered both the ground, "singlet-singlet" state (*i.e.*, dissociating into a pair of singlets) and the first singlet excited state, the "triplet-triplet" state appropriate for $\sigma+\pi$ binding. In keeping with the previous analysis we kept frozen the angle $\angle HSiH$ at its equilibrium value α, and used the energy of a pair of singlets at their equilibrium geometry (α_0) as a reference. The results are reported in Fig. F17b,c where step 1 was followed till the Si-Si seperation took the equilibrium value, $R = R_e = 2.18$ Å. The results show that the ground-state interaction in step 1 is attractive, thereby ruling out the possibility that it keeps its "singlet-singlet" character. Rather, an avoided crossing with the "triplet-triplet" state must occur somewhere between $R \sim 4$ Å and R_e, and allow the $pp(\sigma)$ bond to show up in the ground-state energetics. We checked this with the help of Natural Bond Orbital (NBO) analysis (Fig. F17d,e) that indeed finds a change of character in the ground state electronic structure: a pair of (symmetry equivalent) $n \to p$ bonds is appropriate at large Si-Si distances, while at closer separation two distinct bonds, a σ and a distorted π, emerge. *Trans*-bending stabilizes further the binding in the ground-state and leads to a final *trans*-bent equilibrium structure which, according to NBO analysis, presents a σ and a distorted π bond (Fig. F17f). Interestingly, the same happens in the ^1B_u electronic state, where the odd symmetry with respect to inversion implies some antibonding character in the π bond. This state is indeed analogous to the ^1B_u state of ethylene ($^1B_{1u}$ in D_{2h} symmetry) which is known to be of $\pi\pi^*$ type. Thus, it presents a reduced resistance to bending, as manifested by the

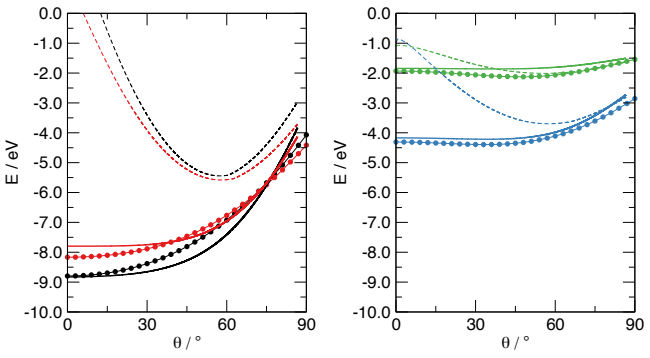

Fig. F16 Pyramidalization energetics in model and in *ab initio* calculations for H_2CCH_2, at fixed $\alpha = 116.50°$, referenced to the singlet-singlet asymptote (see text for details). Solid and dashed lines for the results of the $\sigma+\pi$ and $n-p$ models, respectively, and lines with symbols for B3LYP/6-31++G** *first-principles* data. Left panel for $R_{CC} = R_{eq} = 1.33$ Å (black) and for $R_{CC} = 1.50$ Å. Right panel for $R = 2.00$ Å (blue) and $R = 2.50$ Å (green).

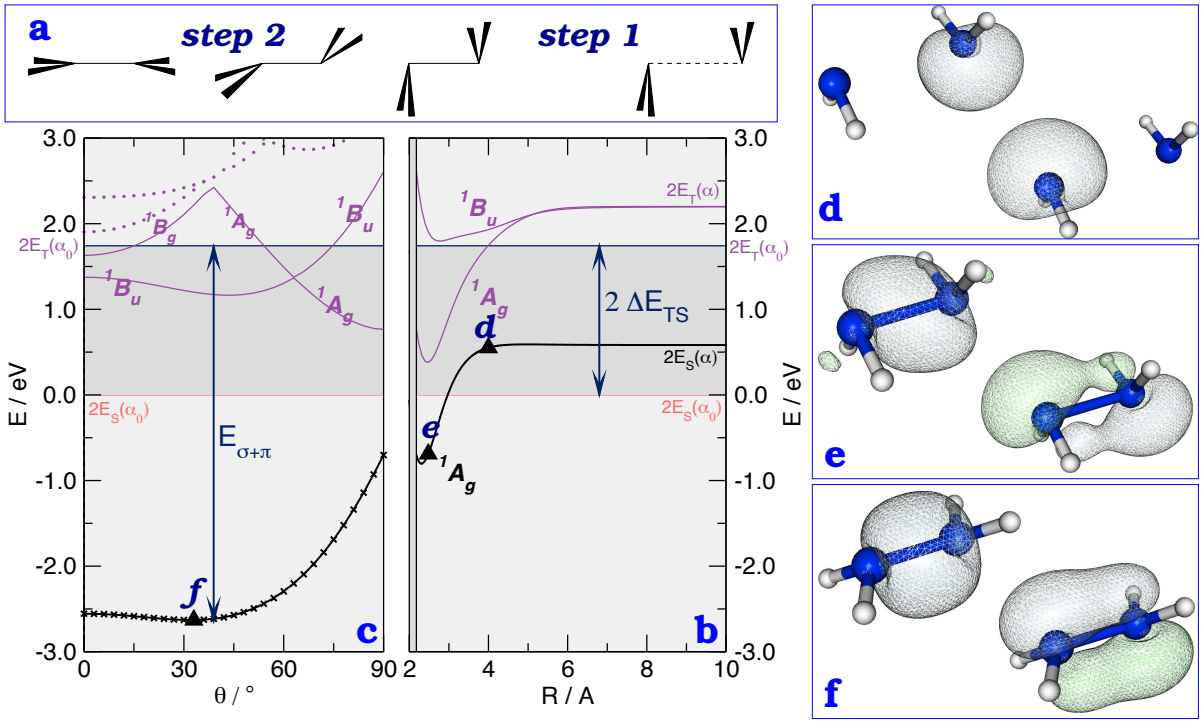

Fig. F17 (a) Schematics of the path considered in the main text. (b,c) DFT energetics along step 1 and step 2, respectively, together with some important energy values: the triplet-singlet separation (E_{TS}) of the fragments and the strength of the double bond ($E_{\sigma+\pi}$). Also shown (purple) are the lowest lying singlet excited states as obtained from linear-responsed TDDFT (solid and dotted lines). In both panels (b) and (c) energy is referenced to the pair of *singlet* fragments in their equilibrium geometry (α_0). (d-f) Relevant (occupied) Natural Bonding Orbitals for the structures (*d-f*) indicated in panels (b) and (c). In (d) the fragments keep their singlet character and the NBOs describe the non-bonding orbitals hosting the lone pairs. In (e,f) the ground electronic state is best described in terms of a σ and a distorted π bond.

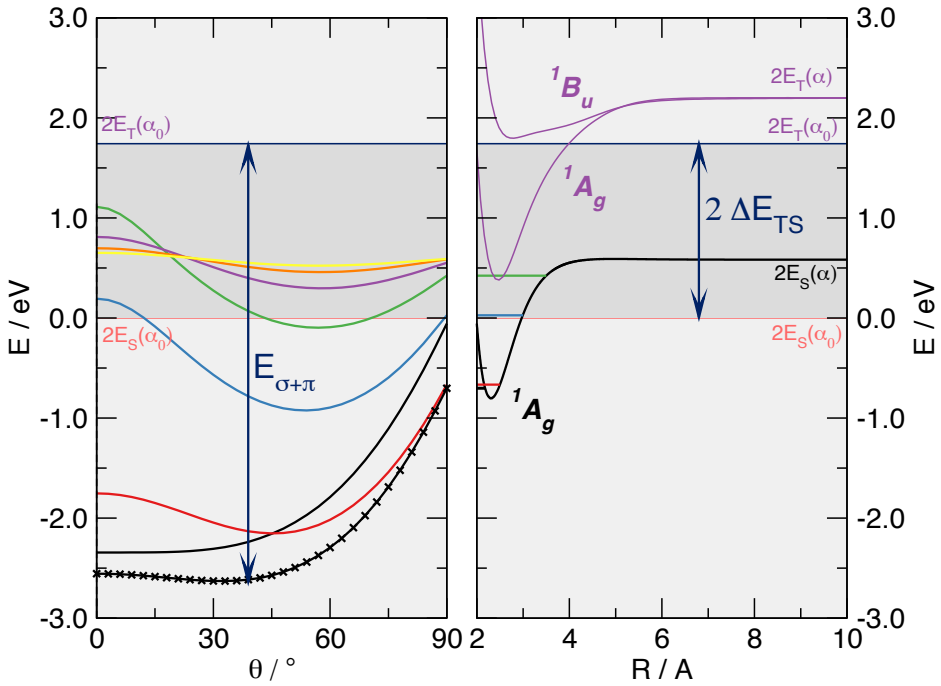

Fig. F18 Energetics of disilene along the path described in Fig. F17, showing the behaviour of *trans*-bending in disilene for different values of the Si-Si distance (R =2.0, 2.5, 3.0, 3.5, 4.0, 4.5 and 5.0 Å as black, red, blue, green, purple, orange and yellow lines in the left panel. Line with crosses for $R = R_{eq}$). Energy is referenced to the pair of *singlet* fragments in their equilibrium geometry (α_0). Purple lines in the right panel are the lowest lying excited states.

deeper minimum in the potential energy curve (violet line in Fig. F17c).

Furthermore, Fig. F18 shows similar results on disilene obtained when bending occurs at different Si-Si separation, R =2.0-5.0 Å in steps of 0.5 Å. The figure shows how bending evolves when stretching the Si-Si bond. Here, $n \rightarrow p$ binding becomes increasingly important, and necessarily dominates at large distances (see also Fig. F15).

Figures F19,F20 report the results of a similar analysis performed on a carbon system (F_2CCF_2) that, even though is not *trans*-bent, has $\Sigma E_{TS} > 0$ and presents a rather small transition length, $R_* \sim$1.5 Å [ethylene pyramidalization energetics was given in Fig. F16, along with model results]. Fig. F19 (left panel) reports the bending energetics at $R = R_{eq}$, when the molecule takes a planar geometry because the π bond resists to pyramidalization. The situation changes in the ^1B_u excited-state that behaves rather similarly to the ground-state but presents a *trans*-bent minimum because of a softer π bond. Increasing the C-C distances makes the ground-state unstable to pyramidalization, consistently with Fig. 3. The main difference with the disilene case considered above is that, in this case, the energetics along step 1 is not flat, rather it shows that the two CF_2 fragments experience a repulsive interaction when they get close to each other in a *trans*-bent arrangement (Fig.s F19,F20, right panels). This is due to the $\pi-$donating effect of the Fluorine atoms on the $p-$like states that, once *e*-doped, partially repel each other, as originally suggested by Trinquier and Malrieu[6]. When *trans*-bent in this way, the molecule prefers the $n \rightarrow p$ binding scheme down to very small distances, according to NBO analysis (Fig. F21, top panel). However this turns into $\sigma + \pi$ as soon as the bending is reduced and a π bond becomes possible. Thus, the *trans*-bent minima of Fig. F20 adopt such kind of bonding scheme (Fig. F21, bottom panel).

Next, we consider the influence of ΣE_{TS} on the distortion. Karni and Apeloig[9] showed long ago how the equilibrium pyramidalization angle in several substitued disilenes correlates linearly with the fragment ΣE_{TS}. We re-consider here this issue using the same theory level adopted in this manuscript, *i.e.* the combination DFT/B3LYP and 6-31++G**, on a selected set of disilenes $YHSiSH_2$. Fig. F22 shows the pyramidalization angle at the HSiH unit (left panel) and the binding energetics (right). For the latter, one distinguishes the "true" binding energy E_{BE} (blue symbols), *i.e.* the energy of the reaction

$$YHSiSiH_2 \rightarrow YHSi(^1A_1) + SiH_2(^1A_1)$$

from the $E_{\sigma+\pi}$ energy (red symbols) which, on the other hand, refers to

$$YHSiSiH_2 \rightarrow YHSi(^3X_1) + SiH_2(^3B_1)$$

As observed by Carter and Goddard on olefines[10], the latter are approximately constant, irrespective of the substituents, in a way that the approximately linear dependence of the former on ΣE_{TS} reflects just the promotion energy, $E_{BE} = E_{\sigma+\pi} - \Sigma E_{TS}$. At a closer look, $E_{\sigma+\pi}$ increases slightly with ΣE_{TS}, probably because the increased $\pi-$donating ability of the species considered destabilizes the triplet fragments more than the molecule and this determines an effective strengthening of the double bond. Importantly, while such relationships suggest a $n \rightarrow p$ binding model, NBO analysis of the equilibrium structures show that in all the cases considered the $\sigma + \pi$ binding scheme seems more appropriate (Fig.s F23,F24). An exception may be Y = NH_2, at the high energy end, where NBO analysis seems to point to two symmetry equivalent bonds of $n \rightarrow p$ type.

S7 Molecular miscellanea

In this section we present some results of the extensive *first-principles* investigations that we performed on a number of model systems. Fig. F25, for instance, shows the structures of typical Si-analogues of PAHs that can be used as silicene surrogate, at least for those properties that are not sensitive to edge effects. The advantage of introducing such models is that they allow, to some extent, the use of sophisticated electronic structure methods that would be computationally prohibitive for extended systems. At the DFT level, this means that a large variety of functionals, comprising (semi)local, hybrid, and hybrid-metaGGA functionals, can be employed. We considered several functionals, and checked them in describing the buckling in Si_6-benzene, Si_{10}-naphatelene and Si_{54}-circumcoronene. The results are reported in Table T1 and, even at a quick look, reveal the importance of electron correlation: at the HF level, buckling is severely underestimated, in accordance with our main findings that correlation plays an important role on pyramidalization.

Fig.s F26 extends the analysis of the main article, and shows the effect of reducing the Coulomb repulsion on a Si_{60}-fullerene. The "true" structure (left panel) is seen to be quite different from a traditional fullerene, and presents several Si atoms that protrud from the "surface". Reduction of Coulomb repulsion (*i.e.*, application of a negative Hubbard on-site energy) gives back the structure that we know from C. With the same token, Fig.s F27 and F28 show the effect of positive charges on buckling, on both standard and "exotic" systems.

Finally, Fig. F29 shows some low energy isomers with structure X_2Y_4 that become more and more relevant when the triplet-singlet fragment energy ΣE_{TS} approaches the $\sigma + \pi$ bond energy ($E_{\sigma+\pi}$). Note that already for Y = H, the isomer SiH_3SiH is (comparatively) much lower in energy than its C counterpart, since the reaction energy of the isomerization $H_2XXH_2 \rightarrow H_3XXH$ decreases from $\sim$ 72.8 kcal mol^{-1} for C to only $\sim$5.5 kcal mol^{-1} for Si. This is suggestive of a very weak π bond in disilene, which is not entirely true because of the subtle role that the spin state of the fragments plays in such context.

S8 The $\sigma + \pi$ model for extended systems

Finally, we describe in this Section how the $\sigma + \pi$ binding model can be extended to describe bonding in extended systems. We consider a honeycomb 2D lattice where each X atoms is surronded by three equivalent atoms and form with them three equal σ bonds using hybrids sp^μ and one π bond using the remaining hybrid sp^λ. If $d_{||}$ is the XX bond length projected on the surface plane ($d_{||} = a/\sqrt{3}$, where a is the lattice constant) and h is the

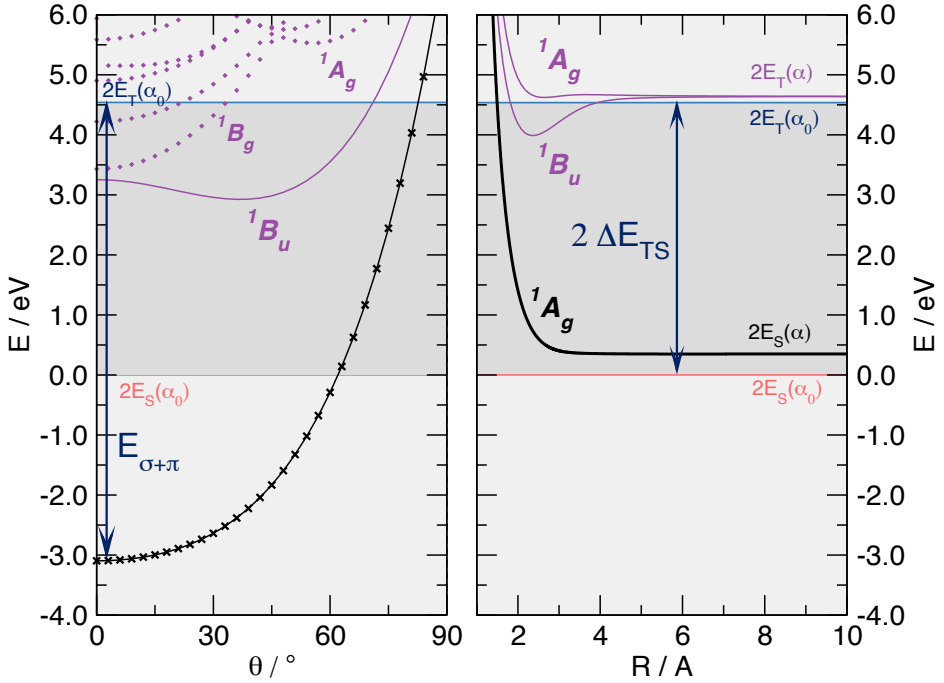

Fig. F19 Same as in Fig. F17, for $F_2C{=}CF_2$. Purple lines are the lowest lying singlet excited states.

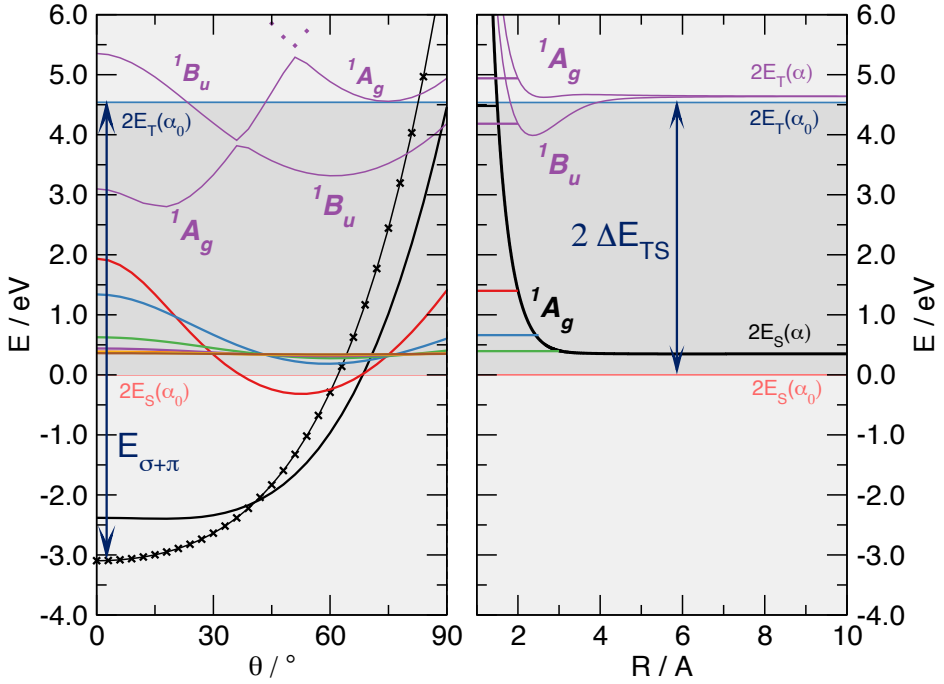

Fig. F20 Same as in Fig. F18, for $F_2C{=}CF_2$. Purple lines on the left panel are the lowest lying singlet excited states at $R = 2.0$ Å.

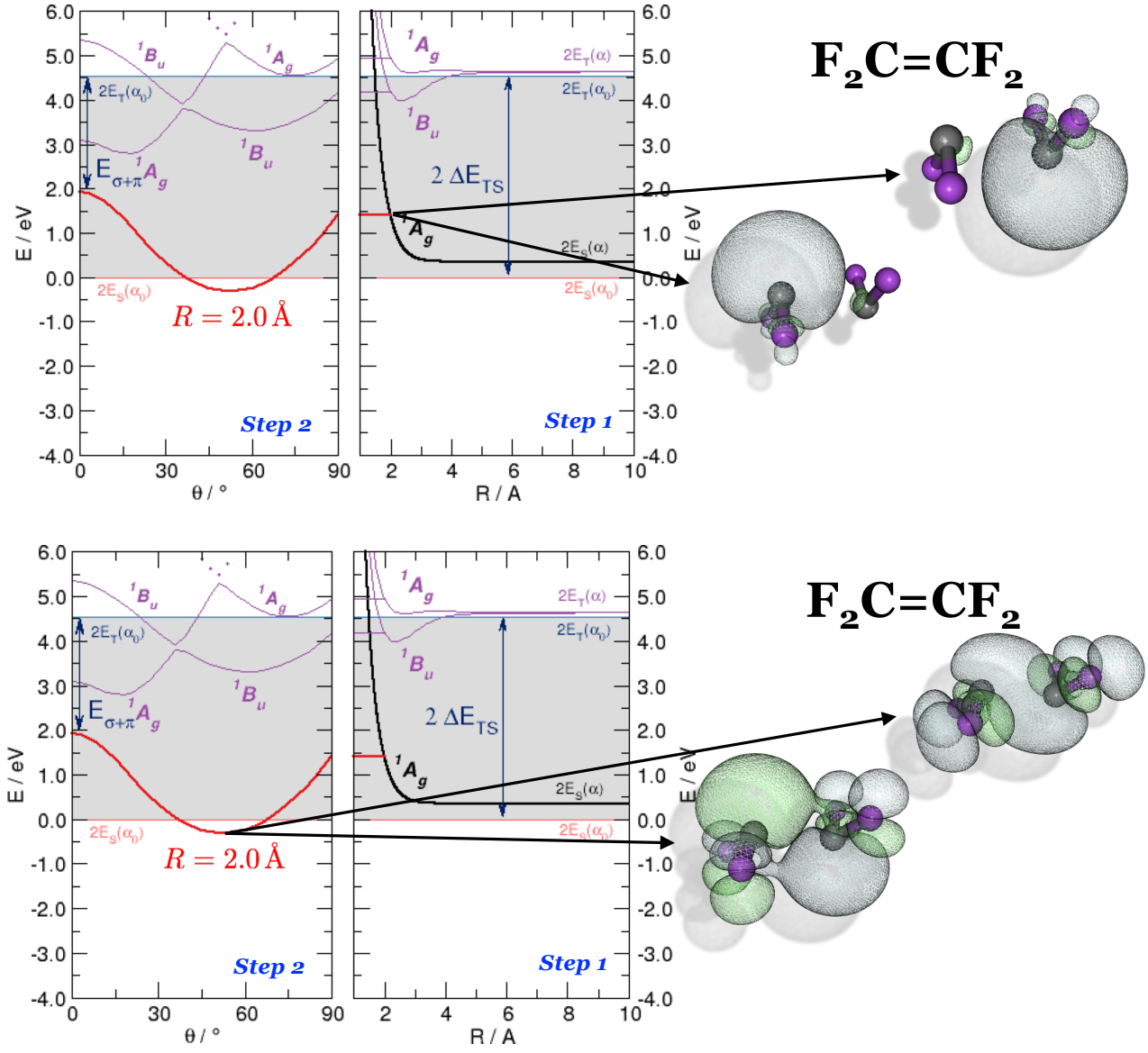

Fig. F21 NBO analysis of two configurations with $R_{CC} = 2.0$ Å, on the top panel for $\theta = 90°$ and on the bottom for the energy minimum θ value.

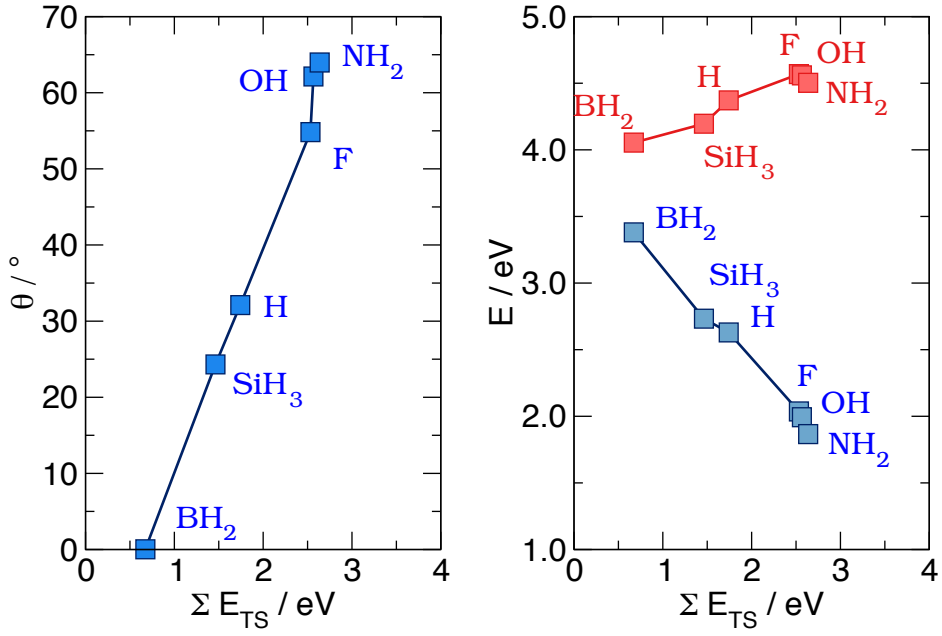

Fig. F22 Left: Equilibrium pyramidalization angle θ in $HYSiSiH_2$ for different species Y, as indicated, *vs.* triplet-singlet separation. Right: corresponding binding (blue) and $\sigma+\pi$ (red) energies.

h / Å	Si_6H_6	$Si_{10}H_8$	$Si_{54}H_{18}$
HF	0.18	0.17	0.18
PBE	0.45	0.44	0.46
B3LYP	0.43	0.41	0.42
M06L	0.40	0.38	0.38
M06	0.48	0.49	0.51
M062X	0.37	0.40	0.42
M06HF	0.33	0.43	0.50

Table T1 Buckling height (h) in the structures of Fig. F25, as obtained with different density functionals and a 6-31++G** basis set. In hexasilabenzene h was determined from the heights of the Si atoms above and below the natural plane, which is midway between the planes defined by up- and down- Si atoms. For Si_{10}−naphatelene and Si_{54}−circumcoronene h was defined similarly but at the center of the molecule only.

buckling height, it is not hard to show that

$$\mu = 2\frac{d_\parallel^2+h^2}{d_\parallel^2-2h^2}$$

is the hybridization index for the hybrids responsible for σ binding ($\theta=\arccos(-1/\mu)$ is the XX angle) and

$$\lambda = \frac{d_\parallel^2}{2h^2}-1$$

is the one for the hybrids involved in the π bonds (note that $\lambda=0$ for $h=d_\parallel/\sqrt{2}=a/\sqrt{6}$, which then represents the maximum value of the buckling height that can be considered). The binding energy then follows as

$$E_{\rm cell} = 3E_\sigma + E_\pi + 3v$$

where $v=v(d)$ is the ion-core repulsive potential, to be evaluated at a distance $d=\sqrt{d_\parallel^2+h^2}$. This binding energy refers to a pair of X atoms in atomic configuration $..(sp^\mu)^3(sp^\lambda)^1$ -energetically equivalent to s^1p^3 - and thus lies at an energy $2(\varepsilon_{sp}-U_{ss}^{\rm eff})$ above the ground-state pair. Hence, the cohesive energy per atom reads as

$$E_{\rm coh} = \frac{3}{2}E_\sigma + \frac{1}{2}E_\pi + \frac{3}{2}v - (\varepsilon_{sp}-U_{ss}^{\rm eff})$$

where the σ and π contribution can be computed as described in Sec.s S1,S2 (Note that, by construction, this expression takes partially into account the resonance phenomenon, in that it represents an *incoherent* average of resonanting structures). This expression can be directly checked against *first-principles* calculations. To this end, we scanned the lattice constant a for X=Si and searched the lowest energy structure for each given a. The results of such investigation (the cohesive energy and buckling height h) are reported in Fig. F30, left and middle panel, where they are compared with the results of different DFT calculations. For the latter, in particular, we considered both plane-wave and atom-centered one-particle sets, *i.e.,* two rather different set-ups that give us confidence about the realiability of such calculations. One sees from Fig. F30 that the $\sigma+\pi$ binding model describes the so-called low-buckled Si-monolayer quite well, in that it predicts a (low) buckled equilibrium structure for $a\sim 3.8$ Å, similarly to the *first-principles* calculations (blue symbols). Both the value of the buckling height (at equilibrium) and of the cohesive energy are reasonably well reproduced, that is not worse than DFT itself when employed with a small (DZP) set. Only for large values of a the model predictions is at odds with the *first-principles* results, since the latter always favor (for both Si and Ge) a buck-

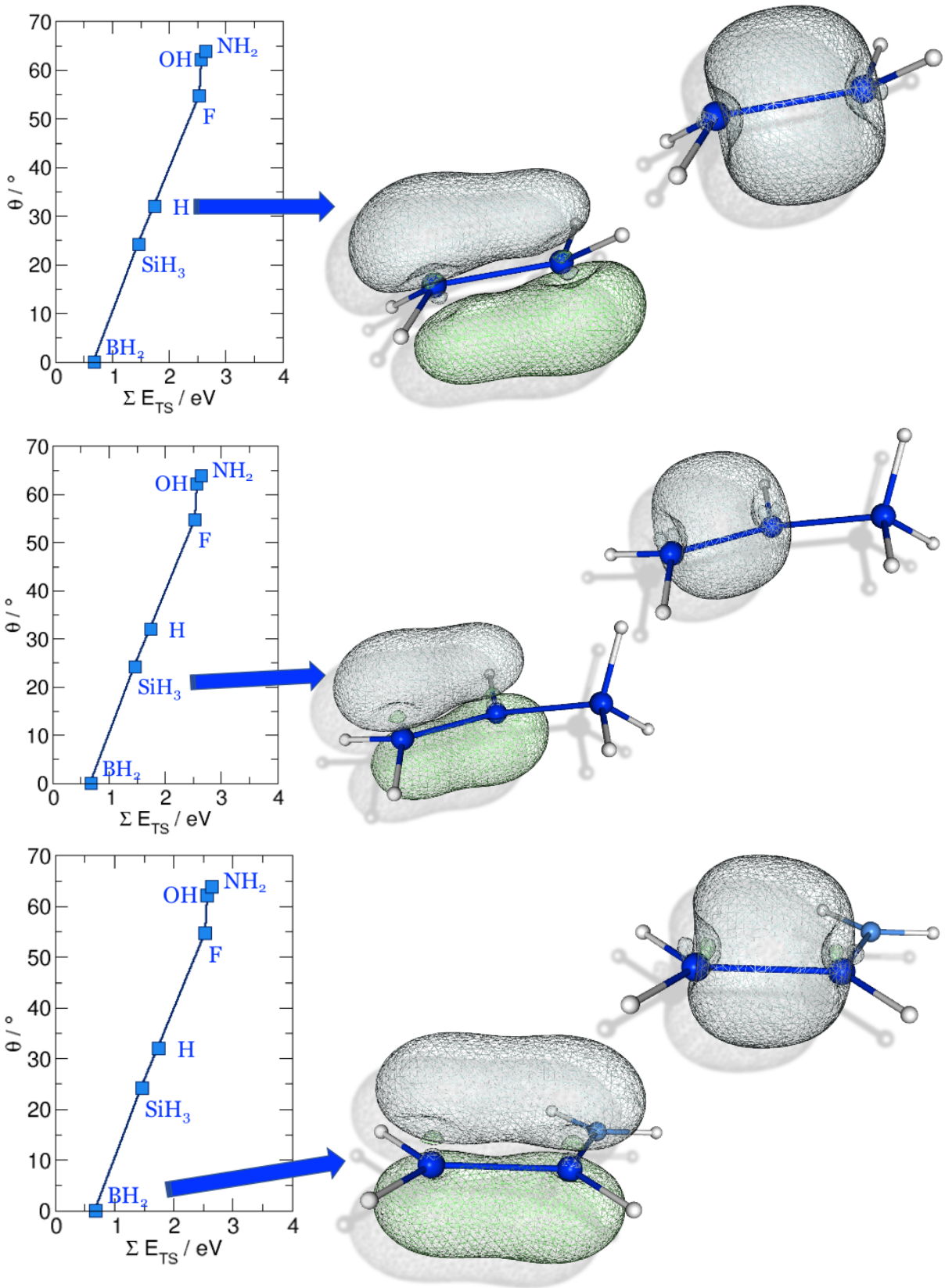

Fig. F23 Natural Bond Orbitals relevant for fragment binding in the disilene structures $HYSiSiH_2$, as indicated.

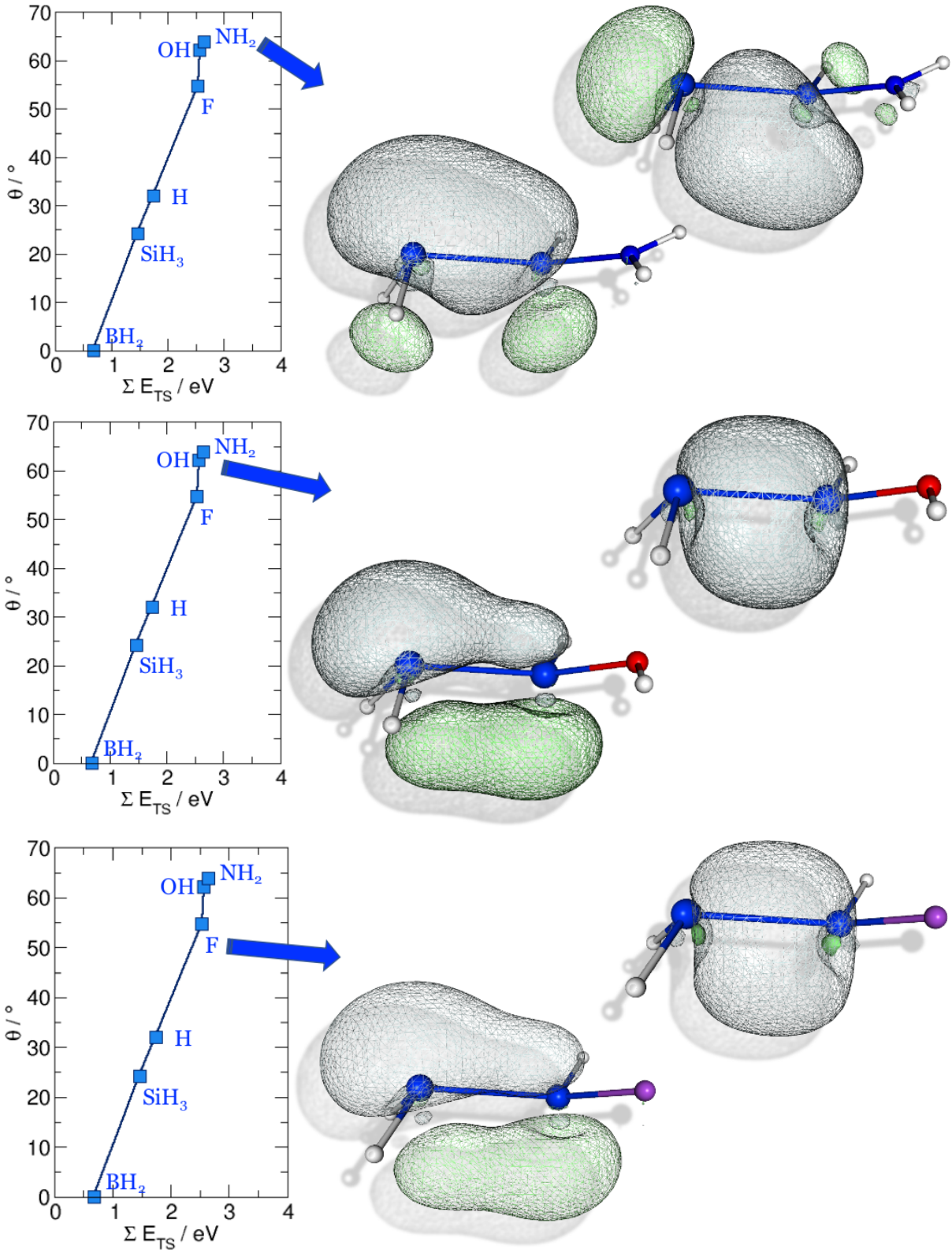

Fig. F24 Natural Bond Orbitals relevant for fragment binding in the disilene structures $HYSiSiH_2$, as indicated.

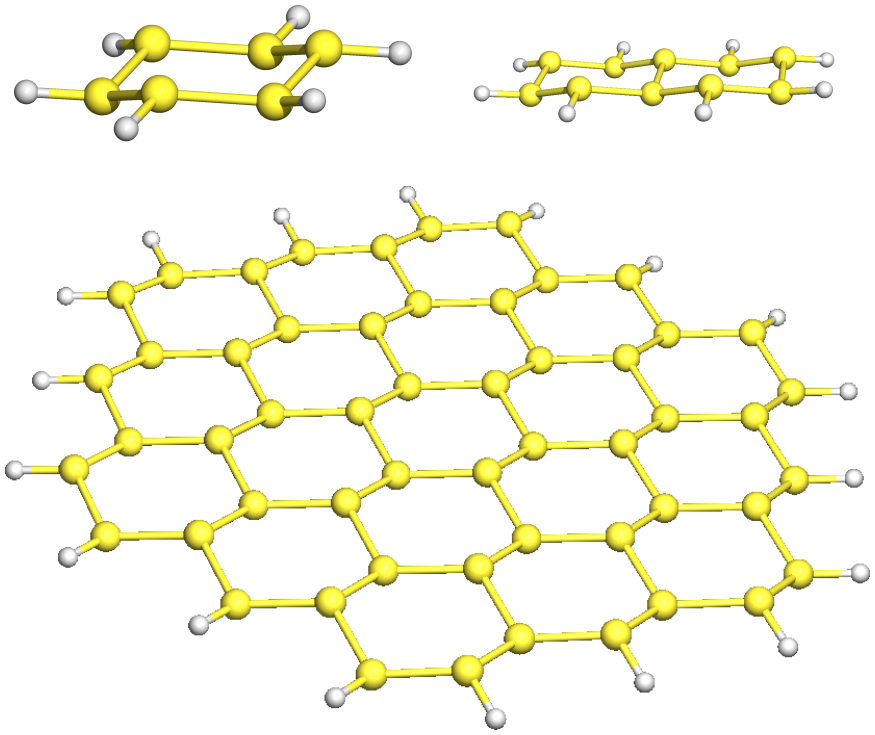

Fig. F25 Optimized structures of hexasilabenzene (top left), $Si_{10}-$naphatlene (top right) and Si_{54}-circumcoronene (bottom).

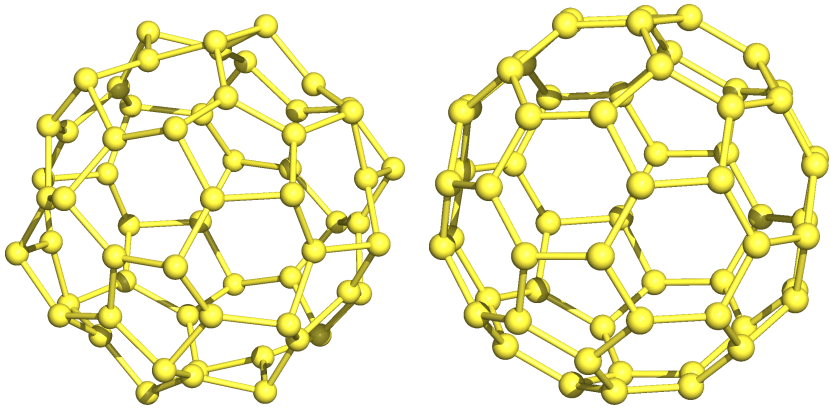

Fig. F26 Optimized structures of Si_{60}-fullerene. Left: PBE results. Right: Hubbard-corrected PBE results, with $\bar{U}$ =-10 eV.

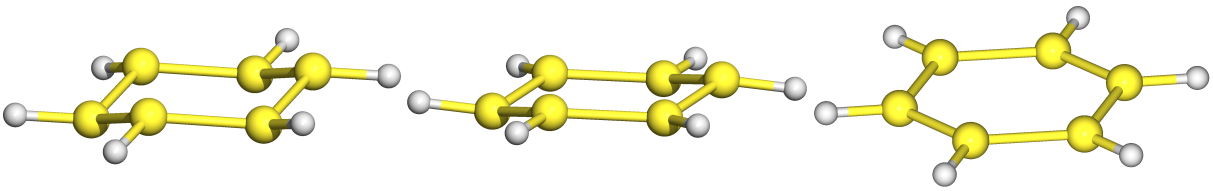

Fig. F27 Optimized structures of hexasilabenzene (left) and its single (middle) and doubly charged (right) cations at the M062X level of theory. From left to right, the buckling height at the M062X/6-31++G** level of theory is 0.37, 0.22 and 0.11 Å, respectively. Hexasilabenzene is found to have six equal SiSi bonds which are 2.220 Å long, while $Si_6H_6^+$ turns out to have two short (2.183 Å) and four long bonds (2.253 Å) and $Si_6H_6^{++}$ four short (2.245 Å) and two long (2.287 Å) bonds.

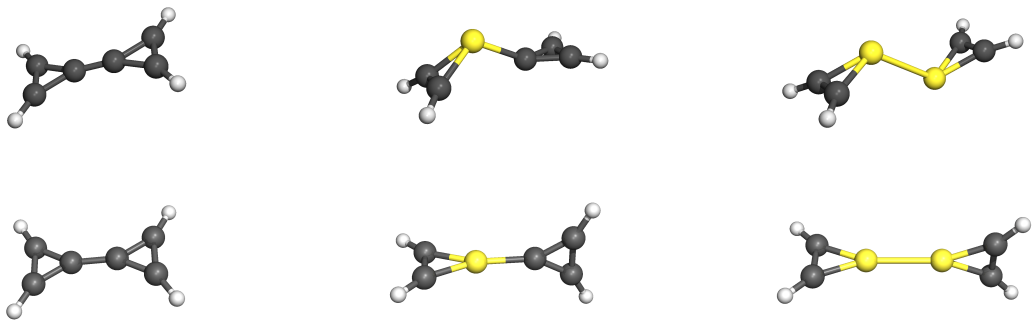

Fig. F28 Optimized structures of 1,1′-dehydro-Bi(cycloprop-2-ene) (left) and its silicon analogues with one (middle) or two (right) Si atoms. Top for the neutral structures and bottom for the doubly charged structures. In the left panels, from top to bottom, the central CC bond stretches from 1.31 to 1.46 Å. In the Si-containing rings, from top to bottom, the SiC bonds shrinks from 1.86 to 1.75 Å for the structures in the middle panels and from 1.84 to 1.76 Å for those on the right.

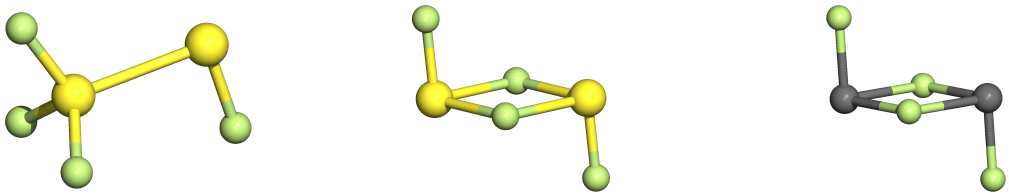

Fig. F29 Optimized structures of some X_2F_4 isomers. On the left panel, the most stable Si_2F_4 isomer, *ca.* 5 kcal mol^{-1} more stable than the double-bridged structure shown in the middle panel. On the right, the most stable Ge_2F_4 isomer.

led rather than flat configuration. This is likely due to the presence of a different bonding scheme that, similarly to the $n \to p$ binding described in Sec. S5, becomes more appropriate at large separations. Fig. F30 (right panel) also shows the behaviour of the buckling height when effectively increasing or reducing the strength of the on-site Coulomb repulsion, in model calculations with Hubbard corrected DFT. The increase (decrease) of buckling when strengthening (weakening) such Coulomb repulsion parallels a decrease (increase) of cohesive energy that is qualitatively well described by the $\sigma + \pi$ model (not shown). Importantly, very similar *first-principles* results are obtained when using rather different level of theory (*i.e.,* very different implementation of the Hubbard correction).

S9 Materials miscellanea

In this Section we describe the results of some representative calculations we performed on extended systems; a detailed account of the results will be provided in a forthcoming publication.

First, as mentioned in the main text, we used Hubbard corrected DFT calculations to tune Coulomb repulsion between the π electrons in elemental monolayers. Fig. F30 (right panel) extends Fig. 5 in that it shows a comparison between two rather different implementation of the Hubbard correction, namely the plane-wave/ PAW set-up discussed in the main text, and available in `ABINIT`, and the atom-centered / PP set-up available in `Siesta`. The main difference between the two is that in the first case the Hubbard term is introduced inside the PAW sphere only, while in the second is applied to a "pseudo-atom" defined by localized AOs. However, as made evident in Fig. F30, the results are rather insensitive to the such details, provided similar parameters (*e.g.,* the range of the pseudo-atomic wavefunctions) are used in both calculations. This gives us confidence on the reliability of the results, and their physical content.

Next, we consider binding in honeycomb layered materials. First of all, we assessed the performance of the PBE functional when adding different variant of the empirical vdW correction, while keeping the layers flat. We computed the "binding potential energy curves" of the multilayers by changing the length of the c axis, which determines the interlayer distance ($d = c/2$), while keeping the in-plane lattice at the equilibrium structure it takes in the monolayer. Fig. F31 shows the resulting cohesive energies (per atom, in meV) for C, Si and Ge structures. The only experimental data to compare with are the cohesive energy of graphite measured by[11] and its c lattice parameter, indicated as black dot in Fig. F31a. From such a comparison, one sees that the van der Waals D3 correction proposed by Grimme[12] and based on the Becke-Jonhson method[13] shows a superior performance than the others, and reproduces both the energy and the equilibrium interlayer distance in graphite quite well. This suggests that for the artificially flat-layer structures of Fig. F31b,c such level of theory is the most reliable. We also checked vdW-inclusive density functionals[14] - presently available only in combination with AO basis-sets[15] - and found qualitatively similar results, but the presence of a basis-set superposition error makes difficult to use some recipe with confidence. A striking difference of the results of F31b,c for Si and Ge, w.r.t. to those reported in F31a for graphene, is the

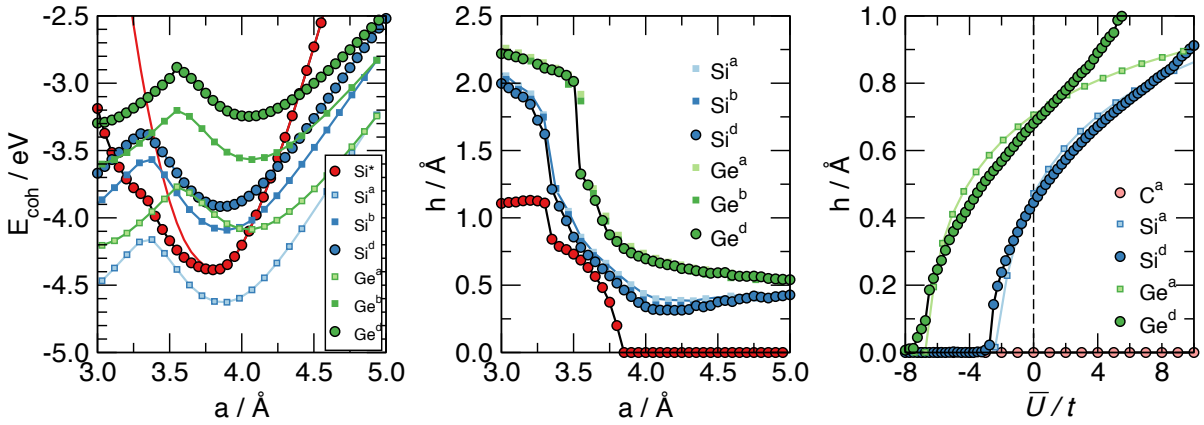

Fig. F30 Si and Ge monolayer structure and energetics. Left: cohesive energy (per atom, eV), for Si and Ge honeycomb monolayers as functions of the lattice constant a, as obtained at different level of DFT theory. Also shown for comparison, for Si only, the results of the $\sigma+\pi$ model described in Sec. S8 (red symbols) and the results of such model for flat monolayers (thin red lines). Middle: monolayer structure for the calculations of the left panel, as described by the bucking height h. Right: buckling height as a function of the on-site Coulomb energy used in DFT+$\bar{U}$ calculations. The DFT calculations are as follows: (a) DZP / PPs (b) TZ2P++ / PP (c) PW / PPs and (d) PW / PAW method, where DZP (TZ2P) denotes an atom centered set with double (triple) splitting and single (double) polarization (++ stands for two diffuse functions), PW denotes a plane-wave calculation, PP stands for norm-conserving pseupotentials and PAW for the projector augemented wave method.

shape and the depth of the binding curves, which suggest the formation, at short distances, of some sort of covalent bond between layers. Such covalent interaction can be reduced (and removed) when reducing the Coulomb interaction between π electrons (*i.e.*, strengthening the intralayer π bonds), as the model calculations with Hubbard corrected functionals show (see left panels in Fig.s F32 and F33). When $\bar{U}$ is given sufficiently negative values the interaction turns to be purely van der Waals, and the structures become stable against buckling. This is seen in the same Fig.s F32 and F33, right panels, where cuts of the potential energy surface are displayed along the buckling coordinate, for interlayer distances close to the minimum energy ones.

Finally, extending the results of Fig. F26 concerning 0D systems, Fig. F34 shows that a reduced Coulomb interaction is effective in flattening structure also in 1D. Fig. F34 shows the evolution of the structure of a simple Si-nanotube when using more and more negative values of $\bar{U}$. Applications of these ideas of several other structures will be presented in a forthcoming publication.

S10 Computational methods

The computational methods used in this work can be briefly summarized as follows.

For molecules, all-electron density functional calculations were performed using the popular B3LYP hybrid functional to describe exchange-correlation effects and the Pople's 6-31++G** atomic-orbital basis-set to expand the Kohn-Sham orbitals, in a spin-unrestricted framework. Calculations were performed with the `Gaussian16` code[16] using generalized internal coordinates to perform constrained geometry optimizations and default tight convergence criteria. Linear-response TDDFT calculations used the same functional in the adiabatic approximation and followed Casida's strategy to compute the excited electronic states, as implemented in the same code.

For extended systems, spin-polarized *first-principles* calculations were performed within the plane-wave PAW approach, as implemented in the `ABINIT` code[17,18]. The JTH PAW dataset[19] and the bare PBE GGA-functional were used throughout, except when investigating layered crystals, for which the van der Waals D3 correction proposed by Grimme[12] (and based on the Becke-Jonhson method[13]) was added. A rather high plane-wave cutoff ($\geq$ 20 Ha) was chosen to ensure tight convergence of the electronic energy w.r.t. the real-space mesh and integrations over the Brillouin zone were performed using a 30×30×1(3) Monkhorst-Pack k-grids for monolayers (multilayers), introducing a large vacuum region (20 Å) when necessary and adopting tight convergence criteria on forces in the geometry optimization runs ($<$ 0.001 eV/Å). DFT+$\bar{U}$ calculations[20,21] used the Hubbard term inside the PAW sphere only, in its fully rotationally invariant form with double-counting correction in the fully localized limit[22], as described in Ref. 23. For comparison, all calculations were also performed with norm-conserving pseudopotentials[24], using the same PBE functional above and either a plane-wave (`ABINIT`) or an atom-centered basis set of double-ζ *plus* polarization quality (`Siesta`[15]). With pseudopotentials, DFT+$\bar{U}$ is available only with AOs and relies on pseudo-atomic wavefunctions. Similarly for vdW inclusive functionals[14], that were used to treat dispersion forces in test calculations, in conjunction with the counterpoise scheme to correct the basis set superposition error.

References

1 F. Aryasetiawan, M. Imada, A. Georges, G. Kotliar, S. Biermann and A. I. Lichtenstein, *Physical Review B*, 2004, **70**, 195104.

2 D. Porezag, T. Frauenheim, T. Köhler, G. Seifert and R. Kaschner, *Physical Review B*, 1995, **51**, 12947–12957.

3 T. Frauenheim, F. Weich, T. Köhler, S. Uhlmann, D. Porezag and G. Seifert, *Physical Review B*, 1995, **52**, 11492–11501.

4 T. O. Wehling, E. Siasoglu, C. Friedrich, A. I. Lichtenstein, M. I. Katsnelson and S. Blugel, *Physical Review Letters*, 2011, **106**, 236805.

5 F. Weinhold and C. R. Landis, *Discovering Chemistry with Natural Bond Orbitals*, John Wiley & Sons, Inc., Hoboken, NJ, USA, 2012.

6 G. Trinquier and J. P. Malrieu, *Journal of the American Chemical Society*, 1987, **109**, 5303–5315.

7 J. P. Malrieu and G. Trinquier, *Journal of the American Chemical Society*, 1989, **111**, 5916–5921.

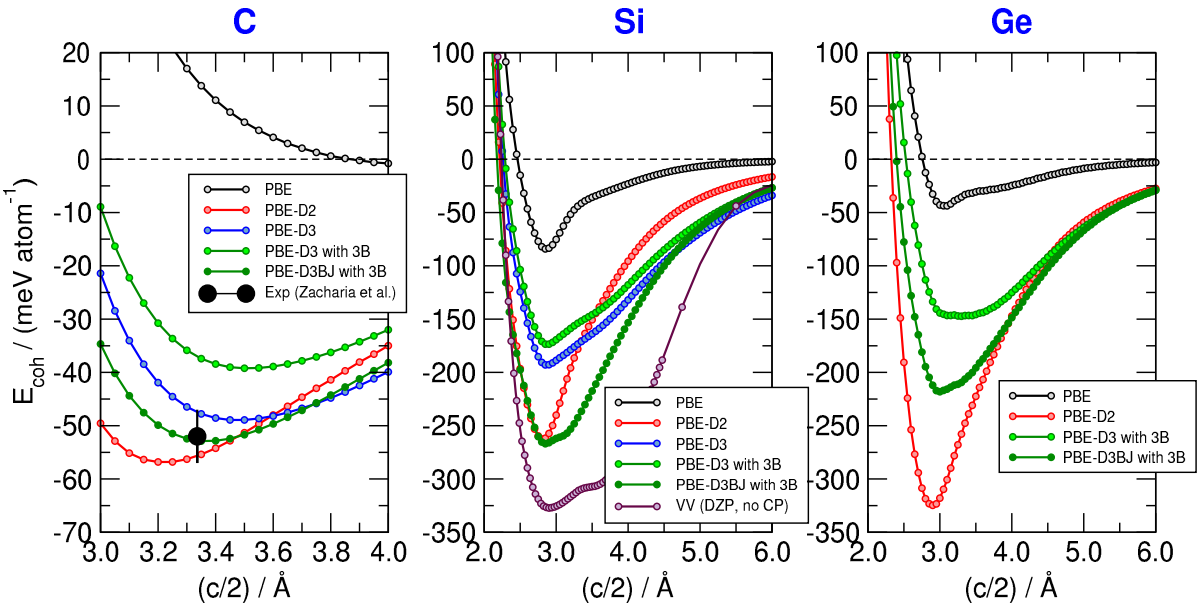

Fig. F31 Interlayer cohesive energy (in meV/atom) in graphite-like, multilayer group-IV structures, at a constrained flat configuration, as a function of the interlayer spacing (half of the c lattice constant). Left, middle and right panels for C, Si and Ge, respectively, at different level of theory. Panel a also shows the experimental value[11].

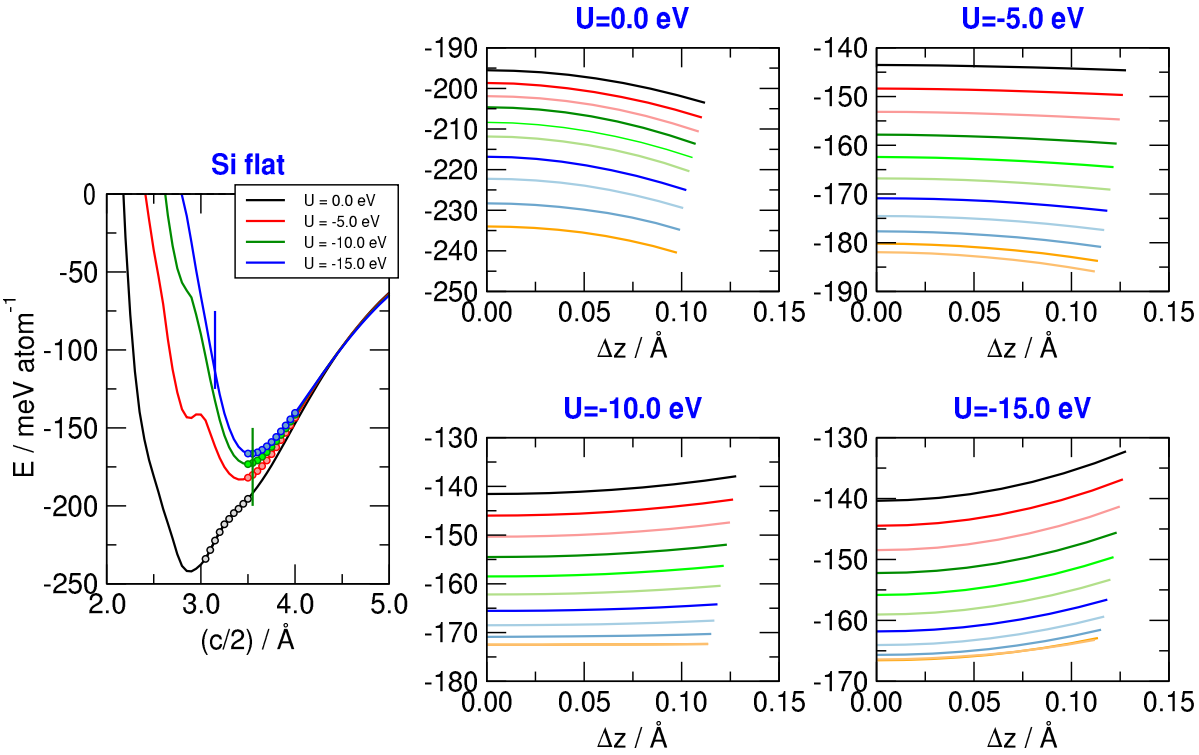

Fig. F32 Interlayer cohesive energy (in meV/atom) in a graphite-like, multilayer structures of Si, as obtained from Hubbard corrected DFT calculations for different values of $\bar{U}$. The left panel shows the energetics for flat layers. The symbols denote the interlayer distances for which the "buckling potentials" have been computed and reported in the right panels, at the different $\bar{U}$ values considered. Vertical bars mark the minimum distance for stable, flat multilayer structures.

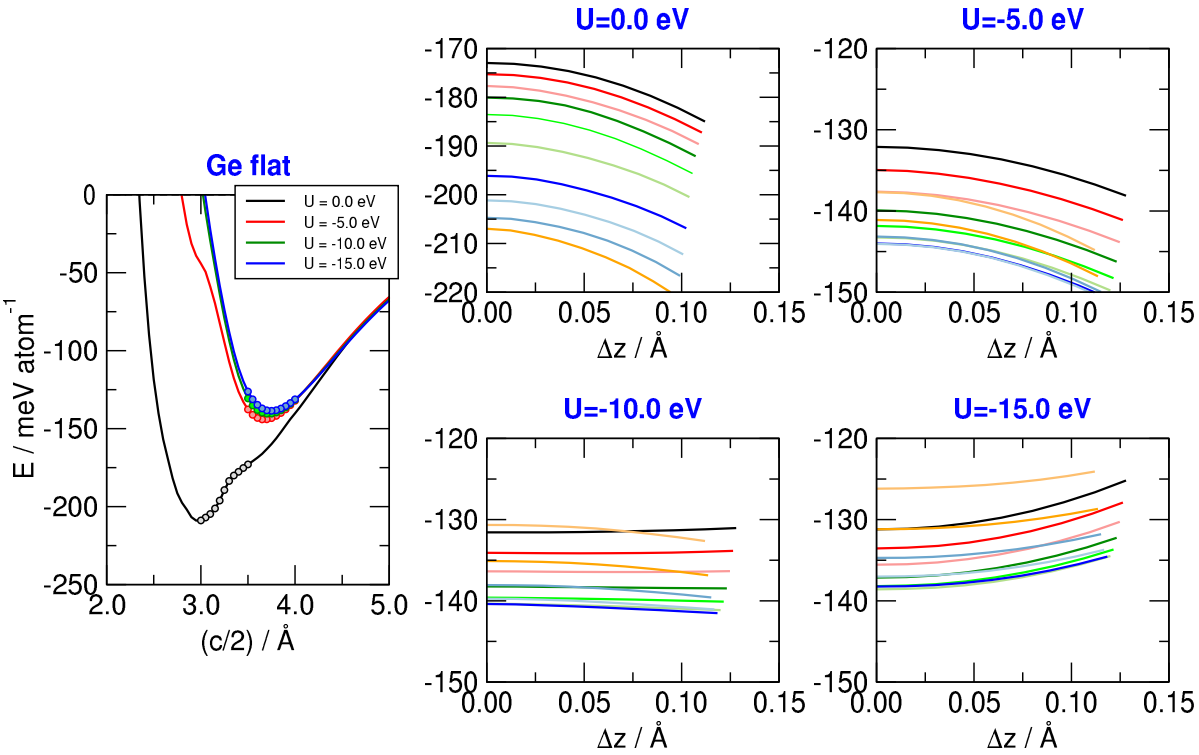

Fig. F33 Same as in Fig. F32, for Ge multilayers.

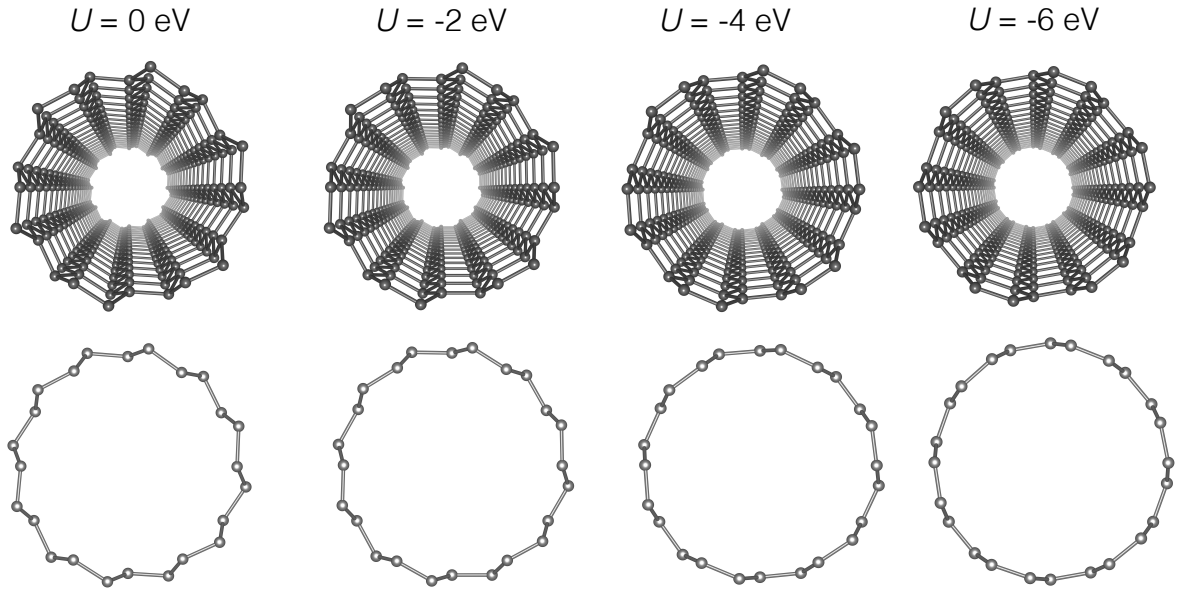

Fig. F34 Structural evolution of a Si-nanotube with chirality $(n,m) = (6,6)$ when reducing the *e-e* repulsion, in model Hubbard-corrected DFT calculations.

8 G. Trinquier and J. P. Malrieu, *The Journal of Physical Chemistry*, 1990, **94**, 6184–6196.

9 M. Karni and Y. Apeloig, *Journal of the American Chemical Society*, 1990, **112**, 8589–8590.

10 E. A. Carter and W. A. Goddard, *The Journal of Physical Chemistry*, 1986, **90**, 998–1001.

11 R. Zacharia, H. Ulbricht and T. Hertel, *Phys. Rev. B*, 2004, **69**, 155406.

12 S. Grimme, J. Antony, S. Ehrlich and H. Krieg, *The Journal of Chemical Physics*, 2010, **132**, 154104.

13 A. D. Becke and E. R. Johnson, *The Journal of Chemical Physics*, 2006, **124**, 221101.

14 M. Dion, H. Rydberg, E. Schröder, D. C. Langreth and B. I. Lundqvist, *Phys. Rev. Lett.*, 2004, **92**, 246401.

15 J. M. Soler, E. Artacho, J. D. Gale, A. García, J. Junquera, P. Ordejón and D. Sánchez-Portal, *Journal of Physics: Condensed Matter*, 2002, **14**, 2745.

16 M. J. Frisch, G. W. Trucks, H. B. Schlegel, G. E. Scuseria, M. A. Robb, J. R. Cheeseman, G. Scalmani, V. Barone, G. A. Petersson, H. Nakatsuji, X. Li, M. Caricato, A. V. Marenich, J. Bloino, B. G. Janesko, R. Gomperts, B. Mennucci, H. P. Hratchian, J. V. Ortiz, A. F. Izmaylov, J. L. Sonnenberg, D. Williams-Young, F. Ding, F. Lipparini, F. Egidi, J. Goings, B. Peng, A. Petrone, T. Henderson, D. Ranasinghe, V. G. Zakrzewski, J. Gao, N. Rega, G. Zheng, W. Liang, M. Hada, M. Ehara, K. Toyota, R. Fukuda, J. Hasegawa, M. Ishida, T. Nakajima, Y. Honda, O. Kitao, H. Nakai, T. Vreven, K. Throssell, J. A. Montgomery, Jr., J. E. Peralta, F. Ogliaro, M. J. Bearpark, J. J. Heyd, E. N. Brothers, K. N. Kudin, V. N. Staroverov, T. A. Keith, R. Kobayashi, J. Normand, K. Raghavachari, A. P. Rendell, J. C. Burant, S. S. Iyengar, J. Tomasi, M. Cossi, J. M. Millam, M. Klene, C. Adamo, R. Cammi, J. W. Ochterski, R. L. Martin, K. Morokuma, O. Farkas, J. B. Foresman and D. J. Fox, *Gaussian16 Revision A.03*, 2016, Gaussian Inc. Wallingford CT.

17 X. Gonze, B. Amadon, P.-M. Anglade, J.-M. Beuken, F. Bottin, P. Boulanger, F. Bruneval, D. Caliste, R. Caracas, M. Côté, T. Deutsch, L. Genovese, P. Ghosez, M. Giantomassi, S. Goedecker, D. Hamann, P. Hermet, F. Jollet, G. Jomard, S. Leroux, M. Mancini, S. Mazevet, M. Oliveira, G. Onida, Y. Pouillon, T. Rangel, G.-M. Rignanese, D. Sangalli, R. Shaltaf, M. Torrent, M. Verstraete, G. Zerah and J. Zwanziger, *Computer Physics Communications*, 2009, **180**, 2582–2615.

18 X. Gonze, F. Jollet, F. Abreu Araujo, D. Adams, B. Amadon, T. Applencourt, C. Audouze, J.-M. Beuken, J. Bieder, A. Bokhanchuk, E. Bousquet, F. Bruneval, D. Caliste, M. Côté, F. Dahm, F. Da Pieve, M. Delaveau, M. Di Gennaro, B. Dorado, C. Espejo, G. Geneste, L. Genovese, A. Gerossier, M. Giantomassi, Y. Gillet, D. Hamann, L. He, G. Jomard, J. Laflamme Janssen, S. Le Roux, A. Levitt, A. Lherbier, F. Liu, I. Lukačević, A. Martin, C. Martins, M. Oliveira, S. Poncé, Y. Pouillon, T. Rangel, G.-M. Rignanese, A. Romero, B. Rousseau, O. Rubel, A. Shukri, M. Stankovski, M. Torrent, M. Van Setten, B. Van Troeye, M. Verstraete, D. Waroquiers, J. Wiktor, B. Xu, A. Zhou and J. Zwanziger, *Computer Physics Communications*, 2016, **205**, 106–131.

19 F. Jollet, M. Torrent and N. Holzwarth, *Computer Physics Communications*, 2014, **185**, 1246–1254.

20 V. I. Anisimov, J. Zaanen and O. K. Andersen, *Physical Review B*, 1991, **44**, 943–954.

21 B. Himmetoglu, A. Floris, S. de Gironcoli and M. Cococcioni, *International Journal of Quantum Chemistry*, 2014, **114**, 14–49.

22 A. I. Liechtenstein, V. I. Anisimov and J. Zaanen, *Physical Review B*, 1995, **52**, R5467–R5470.

23 B. Amadon, F. Jollet and M. Torrent, *Physical Review B*, 2008, **77**, 155104.

24 N. Troullier and J. L. Martins, *Physical Review B*, 1991, **43**, 1993–2006.